Yongzhe Li

# Ambiguity function of the transmit beamspace-based MIMO radar

**School of Electrical Engineering**

Thesis submitted for changing the visiting student status at Aalto University.

Espoo 20.10.2014

**Thesis supervisor and advisor:**

Prof. Sergiy A. Vorobyov

Aalto University
School of Electrical
Engineering

Author: Yongzhe Li

Title: Ambiguity function of the transmit beamspace-based MIMO radar

Date: 20.10.2014 Language: English Number of pages: 8+60

Department of Signal Processing and Acoustics

Professorship: Signal processing technology Code: S-88

Supervisor and advisor: Prof. Sergiy A. Vorobyov

We formulate and investigate an ambiguity function (AF) for the transmit beamspace (TB)-based multiple-input multiple-output (MIMO) radar for the case of far-field targets and narrow-band waveforms. The effects of coherent processing gain and waveform diversity are incorporated into the AF definition. To cover all the phase information conveyed by different factors, we introduce the so-called equivalent transmit phase centers. The newly defined AF serves as a generalized AF form for which the phased-array (PA) and traditional MIMO radar AFs are important special cases. We establish relationships among the defined TB-based MIMO radar AF and the existing AF results including the Woodward's AF, the AFs defined for the traditional colocated MIMO radar, and also the PA radar AF, respectively. Moreover, we compare the TB-based MIMO radar AF with the square-summation-form AF definition and identify two limiting cases to bound its "clear region" in Doppler-delay domain that is free of sidelobes. Corresponding bounds for these two cases are derived, and it is shown that the bound for the worst case is inversely proportional to the number of transmitted waveforms $K$, whereas the best case bound is independent of $K$. The actual "clear region" of the TB-based MIMO radar AF depends on the array configuration and is in between of the worst- and best-case bounds. We also propose a TB design strategy to reduce the level of AF sidelobes, and show in simulations that proper design of the TB matrix leads to reduction of the relative sidelobe levels of the TB-based MIMO radar AF.

Keywords: Ambiguity function (AF), clear region, generalized AF, MIMO radar, transmit beamspace (TB).

# Preface

First of all, I would like to express my most sincere gratitude to my supervisor Prof. Sergiy A. Vorobyov for his high-level guidance, unwavering trust, and strong support in both of my academic research and life. Without his accurate leading of research direction, professional advices on research contents, and active participation in my work, what I have achieved at Aalto University can not become true. He has taught me a lot since my coming to Aalto University in March of 2013 as a visiting Ph.D. student, through research discussions, courses he has provided, and free talks between us. I have to say that I am really lucky to be his student.

I would like to express my sincere gratitude to Prof. Visa Koivunen who has been my second supervisor during my visiting study at Aalto University. He has provided a lot of timely and precious technical comments on my research papers during the past time, and has financially supported me to participate in ICASSP 2014 conference.

The students in the research group of Prof. Visa Koivunen are acknowledged for their kindly acceptance and friendly help.

This work is achieved by collaborating with Prof. Sergiy A. Vorobyov and Prof. Visa Koivunen during my visiting doctoral study at Aalto University. It belongs to the work of my doctoral study. The reason why this thesis is written is to meet the requirement of Aalto ELEC Doctoral Programme Committee in order to change my visiting status at Aalto University.

Otaniemi, October 20, 2014,

Yongzhe Li

# Contents

# List of symbols

| Symbol | Description |
|---|---|
| $(\cdot)^*$ | Conjugate operator |
| $(\cdot)^T$ | Transpose operator |
| $(\cdot)^H$ | Conjugate transpose operator |
| $\|\cdot\|$ | Euclidean norm |
| $\|\cdot\|$ | Absolute value |
| $\otimes$ | Kronecker product |
| $\odot$ | Element-wise product |
| $\mathbb{E}\{\cdot\}$ | Expectation operator |
| $B$ | Radar bandwidth |
| $\mathbf{C}$ | Transmit beamspace matrix |
| $E$ | Total transmit energy within one radar pulse |
| $K$ | Number of transmit beams |
| $M$ | Number of transmit antenna elements |
| $N$ | Number of receive antenna elements |
| $T$ | Pulse duration |
| $t$ | Continuous fast-time index |
| $\varsigma$ | Slow-time index |
| $f_s$ | Sampling frequency |
| $f_c$ | Carrier frequency |
| $\mathbf{\Omega}$ | Spatial angular sector-of-interest |
| $\boldsymbol{\phi}(t)$ | Waveform vector |

# List of abbreviations

| Abbreviation | Description |
|---|---|
| **2D** | Two-dimensional |
| **3D** | Three-dimensional |
| **AF** | Ambiguity function |
| **CRB** | Cramér-Rao bound |
| **DOA** | Direction-of-arrival |
| **DOFs** | Degrees of freedom |
| **LFM** | Linear frequency modulation |
| **GLRT** | Generalized likelihood ratio test |
| **GMTI** | Ground moving target indication |
| **MIMO** | Multiple-input multiple-output |
| **MSE** | Mean-square error |
| **PA** | Phased-array |
| **RIP** | Rotational invariance property |
| **SDP** | Semi-definite programming |
| **SINR** | Signal-to-interference-plus-noise ratio |
| **SNR** | Signal-to-noise ratio |
| **SOCP** | Second-order cone programming |
| **STAP** | Space-time adaptive processing |
| **TB** | Transmit beamspace |

# List of figures

# 1 Introduction

## 1.1 Background

The multiple-input multiple-output (MIMO) radar [1–6], has become the focus of intensive research in recent years. Despite the benefits such as improved parameter identifiability and angular resolution, increased upper limit on the number of resolvable targets, and extended array aperture by virtual sensors, the traditional MIMO radar with colocated transmit antenna elements suffers from the loss of coherent processing gain that can be achieved in the phased-array (PA) radar system. This is due to the omnidirectional transmission of mutually orthogonal waveforms in the traditional MIMO radar configuration. To compensate for this effect, the work of [7] attempts to simultaneously incorporate the benefits of waveform diversity and coherent processing gain by separating the transmit antenna array into several uniform subarrays, and enabling each one to perform as a PA. Unlike [7], the transmit beamspace (TB)-based MIMO radar (see for example [8]) focuses the energy of multiple transmitted orthogonal waveforms within a certain spatial sector where a target is likely to be located using beamspace design techniques. In this radar configuration, beams that fully cover the sector-of-interest are synthesized at the transmitting end. Each beam associated with a certain orthogonal waveform is implemented via the whole transmit array of the TB-based MIMO radar. The essence of it is to find the jointly optimal scheme that achieves improved signal-to-noise ratio (SNR) together with increased aperture by means of TB processing techniques [8–16]. For example, it allows to achieve coherent processing gain or desired beampattern by appropriate design of waveform correlation matrix [9, 10].

Compared to the traditional MIMO radar, one verified benefit of the TB-based MIMO radar is the superior direction-of-arrival (DOA) estimation performance in a wide range of SNRs [8, 12, 13]. Based on the classic approach of *Multiple Signal Classification* (MUSIC) [17] or *Estimation of Signal Parameter via Rotational Invariance Techniques* (ESPRIT) [18], multiple efficient algorithms that facilitate DOA estimation can be developed. Moreover, the Cramér-Rao bound (CRB) derived for the TB-based MIMO radar in [8] demonstrates that it can achieve a lower CRB with fewer waveforms than the traditional MIMO radar with full waveform diversity, and the lowest CRB can be achieved with proper TB design. This leads to emitting non-orthogonal or correlated waveforms from different transmit antenna elements. To study the performance of these actually emitted waveforms as well as the resolution

performance of the TB-based MIMO radar system, it is essential to employ ambiguity function (AF) [19–23] for the performance evaluation.

The well-known Woodward's AF [19, 20], which characterizes the resolution property in Doppler-delay domain for narrow-band waveforms, has served as a starting point for the works on the traditional MIMO radar AF [21–23]. It has been extended to the traditional MIMO radar setup in [21] for the first time, and four AF simplifications corresponding to different scenarios have been derived there. Some properties of the traditional MIMO radar AF have been studied in [22]. Another AF definition for the traditional MIMO radar which does not consider the phase information, has been introduced in [23]. However, with the development of TB design techniques, which allow for non-orthogonal or correlated waveforms to be emitted from each transmit antenna element, the traditional MIMO radar AFs are no longer applicable for the TB-based MIMO radar. This motivates us to derive the AF for the TB-based MIMO radar and investigate how it behaves. Moreover, in-depth study of the TB-based MIMO radar AF also provides insights into the clutter/interference mitigation in airborne MIMO radar system with TB design because Doppler processing of moving target is needed in airborne mode. On the other hand, it is known that the so-called "clear region" [19, 20] denotes the volume-clearance area in Doppler-delay domain which is free of sidelobes. It serves as a measure to determine how close to the ideal thumbtack-shape AF one can come. It is also of great significance for the TB-based MIMO radar AF analysis to see how large its "clear region" is. The work in [23] defines the traditional MIMO radar AF as the sum of the squared noise-free outputs after matched filtering to the waveforms. Based on this definition the "clear region" bound is derived. Such bound is also important to derive for the TB-based MIMO radar AF.

## 1.2 Contributions

In this thesis, we derive the AF for the TB-based MIMO radar. It serves as a generalized AF form for which the existing traditional MIMO radar AF and PA radar AF are important special cases. The effects of both coherent processing gain and waveform diversity are considered when defining the new AF for the TB-based MIMO radar. The phase information conveyed by multiple factors such as array geometry and relative motion is incorporated. Considering that it is impossible to give an exact "clear region" bound for the TB-based MIMO radar AF because the self-transform [19] of the TB-based MIMO radar AF can not guarantee the

non-negativity in general, we identify two limiting cases to conduct the analysis.

The main contributions of this thesis are as follows:

- We review the state of the art in MIMO radar, including the aspects of waveform design, transmit beamforming, parameter estimation and detection, interference suppression, etc. The radar AF works such as Woodward's AF and MIMO radar AF(s) are also reviewed.

- We introduce a new AF definition for the TB-based MIMO radar for the case of far-field targets and narrow-band waveforms. Equivalent transmit phase centers are introduced in the definition as well.

- We show that the TB-based MIMO radar AF is a generalization of AF for many well-known radar configurations such as the PA radar, the traditional MIMO radar (with subarrays), and the TB-based MIMO radar. The AF for each of these radar configurations can be obtained by properly selecting the TB matrix and the equivalent transmit phase centers.

- We establish the relationships among the defined TB-based MIMO radar AF and other existing AFs in the literature including the well-known Woodward's AF, the traditional MIMO radar AF, and the PA radar AF, respectively.

- We compare the newly defined TB-based MIMO radar AF with the square-summation-form AF [23], and propose a TB design strategy to reduce the relative sidelobe levels of the TB-based MIMO radar AF.

- We identify the worst and the best limiting cases for the TB-based MIMO radar AF, and derive the corresponding "clear region" bounds.

## 1.3 Organization of the thesis

The thesis is divided into seven chapters. Chapter 2 presents the overview of MIMO radar and radar AF. Chapter 3 presents the signal models of the traditional and TB-based MIMO radars as well as some preliminaries of TB design. Chapter 4 proposes a newly defined TB-based MIMO radar AF and presents some interesting relationships with other AF works. The "clear region" analysis of the TB-based MIMO radar AF is provided in Chapter 5. Our simulation results are summerized in Chapter 6. Finally, the thesis is concluded in Chapter 7.

# 2 MIMO radar and AF

In this chapter, the overview of MIMO radar and radar AF is presented. The MIMO radar overview, which includes the concept, the categories, and the research status of MIMO radar, is provided in the first section, while the well-known Woodward's AF and the AF works developed for MIMO radar are introduced in the latter section.

## 2.1 MIMO radar overview

### 2.1.1 Concept of MIMO radar

The idea of "MIMO" has been used in communication area to increase the data throughput and link range without additional bandwidth or extra transmit power [24, 25]. Introducing this idea to the field of radar, the concept of MIMO radar simply means that there are multiple radiating and receiving sites. Different from the PA radar system that emits an identical waveform, MIMO radar emits multiple probing signals through its transmit antennas. When the concept of MIMO radar was initially developed, the signals were referred to as mutually orthogonal waveforms. This restriction wa updated later, i.e., non-orthogonal or correlated waveforms were allowed to be transmitted.

The development of MIMO radar dates back to the 1990s when the concept of *Synthetic Impulse and Aperture Radar* (SIAR) [26] was first proposed by the French aerospace research agency ONERA. SIAR transmits narrow-band orthogonal waveforms via omnidirectional antennas. It can achieve the advantage of improved range resolution as wide-band radar due to the capability of synthesizing impulse operation. This type of radar configuration has parallels with MIMO wireless communication systems, and it hence serves as the prototype of MIMO radar.

### 2.1.2 Categories of MIMO radar

According to the antenna configurations of MIMO radar, it can be divided into two categories. One is referred to as widely separated MIMO radar (also named statistical MIMO radar). The other is referred to as colocated MIMO radar (also named coherent MIMO radar). In the former type of MIMO radar, the transmit array elements (and the receive array elements) are broadly spaced, which provides independent scattering responses of a target for each transmit-receive antenna pair. While in the latter type of MIMO radar, the transmit array elements (and the receive

array elements) are closely spaced, which enables the MIMO radar system to share the same spatial angle of a far-field target, i.e., the same scattering response of a far-field target is obtained.

### 2.1.3 Research status of MIMO radar

With continuous efforts in the past decade, researchers have achieved many useful theoretical results about MIMO radar. The research on MIMO radar with widely separated antennas has shown that improved target detection performance, enhanced ability to combat signal scintillation, and more accurate parameter estimation of moving targets can be achieved in this type of MIMO radar configuration [2, 4, 27]. As for the MIMO radar with colocated antennas, it has been shown that it enables improved spatial resolution, better parameter identifiability, increased upper limit on the number of detectable targets, and extended array aperture by virtual arrays [3, 8, 11, 28, 29]. Parts of these advantages of both types of MIMO radar have been concluded in two overview articles [2, 3] published in the early time after the establishment of MIMO radar. There are also discussions about the comparison or relationship between (colocated) MIMO and PA radars [30–32]. The claimed advantages of MIMO radar versus PA radar have been evaluated from a system engineering viewpoint [30]. In short, it is well understood that tradeoffs exist in MIMO radar [11, 33].

The reported literature of MIMO radar starts since the year of 2003. During the first two years, several initial works on MIMO radar were published [5, 29, 34]. For example, degrees of freedom (DOFs) and resolution of MIMO radar have been studied in [29]. It is revealed that (colocated) MIMO radar possesses more DOFs than PA radar, and improved resolution can be obtained. An example of the benefits of MIMO radar has been discussed in the context of space-time adaptive processing (STAP) [35, 36] for ground moving target indication (GMTI) [37]. The work [5] has investigated the performance of (widely separated) MIMO radar from the viewpoint of capitalizing on the target scintillations where the system performance analysis in terms of CRB has also been carried out.

The above-mentioned pioneering works have encouraged researchers to extend MIMO radar research to different branches, including waveform design, transmit beamforming, parameter estimation and detection, interference suppression, etc. A large number of meaningful results related to these fields have been achieved in the past decade, and new interesting results are continuing to emerge in recent years. In the following, the results achieved in these fields are reviewed, and after that, some

current important research issues in MIMO radar area are introduced.

#### 2.1.3.1 Waveform design

Many research works have been devoted to the waveform design in MIMO radar [38–56]. The criteria such as CRB, mutual information, mean-square error (MSE), and AF have been employed in some of the waveform designs. Among all the designs, convex optimization [57] techniques are the most frequently used.

In the earliest reported literature [38], two types of waveform optimization strategies have been studied in the context of static radar environment. One is the image-domain adaptive waveform design, while the other aims at designing for angle estimation in clutter-free environment in which CRB has been firstly exploited. The work of [42] has extended the second waveform design of [38] to a general case of multiple targets in the presence of spatially colored interference and noise. CRB matrix has also been used, and minimization of the trace, the determinant, and the largest eigenvalue of the CRB matrix have been employed as the design criteria there. It has been found that the CRB of parameter estimation is related to the cross-correlation matrix of transmitted waveforms. The joint optimization of waveforms and receiving filters for the case of extended targets in clutter has been considered in [46]. Another joint transmitted waveforms and receiving filter optimization design (for example, for radar imaging) can be found in [45]. The work of [40] has proposed to design the waveforms by maximizing the conditional mutual information between the random target impulse response and the reflected waveforms or minimizing the MSE in estimating the target impulse response. It has been shown that these two criteria lead to the same solution under equal total power constraint. Mutual information based MIMO radar waveform design can also be found in [49].

Designing MIMO radar waveforms based on the AF serves as another way to achieve the goal of obtaining desired waveforms. Intuitively, excellent AF of a certain radar configuration (one or more waveforms may be used) is expected to have a very high peak at its mainlobe but particularly low levels at its sidelobes. In other words, the ideal design with a thumbtack-shape AF is used as a reference to evaluate the quality of waveforms that have been designed. Several works have defined the AF for MIMO radar [21, 23, 58]. In [21], the well-known Woodward's AF [59] has been extended to MIMO radar for the first time. Based on a similar AF definition as in [21], the work of [43] has proposed the design for frequency-hopping waveforms.

Researchers have also employed space-time coding techniques to design MIMO radar waveforms [39, 44, 48]. For example, polyphase-coded waveforms have been

generated using statistical genetic algorithm in [39]. In [44], the classes of waveforms such as *code division multiple access* (CDMA), *time division multiple access* (TDMA), and *frequency division multiple access* (FDMA) waveforms have been studied for MIMO radar, and the way of generating waveforms that facilitate higher adaptive performance of clutter mitigation has been presented. Space-time coding techniques that aims at suppressing the cross-correlation effects of waveforms in MIMO radar have also been studied in [48], where the conditions for removing waveform cross-correlation have been provided. An alternate space-time coding approach, which utilizes conventional radar waveforms and achieves the orthogonality by phase coding among slow-time pulses, has been proposed in [41].

There are also robust [51] and correlated [56] waveform designs for MIMO radar. Some of the relevant research has also chosen to design the cross-correlation matrix of waveforms instead of designing exact waveforms for MIMO radar [9, 10]. The specific designs of this matrix mainly depend upon the goals that need to be achieved. For example, desired (possibly flat) beampattern with a certain width may be required. The corresponding design is also called transmit beamspace design [8, 12–14] due to the reason that it belongs to the category of transmit beamforming. This technique is reviewed in the following sub-subsection.

#### 2.1.3.2 Transmit beamforming

Beamforming is another important research aspect in MIMO radar. Among all the relevant research directions, transmit beamforming (or TB design) [7–14, 60–71] is the most popular subject.

The study of transmit beamforming dates back to the year of 2004 when the innovative work of [60] was published. A method based on gradient search to achieve or approximate the desired spatial transmit beampattern using partial signal correlations has been proposed there. This type of transmit beamforming with arbitrary waveform cross-correlation matrix has been fully studied in the subsequent work [9]. Constrained convex optimization problem has been formulated in order to find the cross-correlation matrix. The work of [10] has studied the transmit beamforming problem in [60] using similar mathematical approach (i.e., convex optimization design). Semidefinite quadratic programming [57] has been employed to solve the beampattern matching design problem. Several beampattern matching criteria including maximization of incident power on multiple targets with known/unknown locations, minimization of beampattern sidelobe levels, and matching to a desired beampattern (i.e., minimizing the difference) have been proposed in [10].

There are also other ways of designing the waveform cross-correlation matrix for the purpose of achieving desired transmit beampatterns [61–64]. The main difference among these methods is that their goals are different. For example, the beampattern ripples within the energy focusing region and the transition bandwidth has been the main considerations in [61], while attentions of signal-to-interference-plus-noise ratio (SINR) and beampattern sidelobe levels have been paid to the design in [64]. In addition, some of these works have proposed to achieve the goal of transmit beamforming by making the design unconstrained [62] or deriving closed-form solutions to the design [63].

In contrast to the above-mentioned transmit beamforming design based on the waveform cross-correlation matrix (or the set of signals), some researchers have taken a more fruitful point of view which involves beamforming vector to achieve the same goal [8, 12–14, 66]. In essence, this type of design is equivalent to the type of that with waveform cross-correlation matrix, but are more flexible and insightful. Initially orthogonal waveforms are assumed to be employed in this type of designs, and waveform correlations (or equivalently, correlated waveforms) are generated by the designed beamforming matrix which is composed of a certain number of beamforming vectors. Moreover, a significant fraction of these methods have been designed aiming at facilitating direction finding or achieving superior DOA estimation performance [8, 12–14].

In [8], two transmit energy focusing designs have been proposed. The first design (named spheroidal sequences-based design) pursues to find the orthogonal basis of the transmit beamspace from the viewpoint of subspace decomposition, while the second one (named convex optimization-based design) casts the design as a convex second-order cone programming problem in which desired phase rotation terms for ESPRIT DOA estimation are involved. It has been shown in [8] that superior DOA estimation performance to that of the traditional MIMO radar (without TB design) can be achieved, and properly selecting the number of transmitted waveforms (or the number of beamforming vectors) can lead to an optimum/lowest CRB of DOA estimation. Another TB design which enables search-free ESPRIT DOA estimation has been proposed in [12]. A specific structure which separates the TB matrix into two conjugate flipped groups has been imposed in order to maintain the rotational invariance property (RIP) [72, 73] for ESPRIT. This TB strategy also belongs to the category of convex optimization-based designs, and it shows superior DOA estimation performance to that of [8]. The reason lies in the fact that better RIP is maintained by this design. The TB-based designs have been shown to be efficient for

the generalization to two-dimensional (2D) transmit arrays [69, 70]. In addition, the work of [66] has studied the TB design from the viewpoint of target tracking. Both the single-target and multiple-target cases have been considered there.

Besides the way of designing the waveform cross-correlation matrix or TB matrix, transmit beamforming has also been implemented via subarrays or subapertures [11, 67, 68]. For example, the work of [11] has proposed the concept of phased-MIMO radar which combines the advantages of both PA and MIMO radars by partitioning the transmit array into several (uniform or overlapped) subarrays. Each subarray performs as a PA radar, and orthogonal waveforms are transmitted individually by different subarrays. It has been shown that the main introduced benefit is that both the coherent processing gain and the waveform diversity at the transmitting end are achieved. Indeed, MIMO radar with subarrays also reduces the required time of coherent integration if the mode of pulse-Doppler processing is employed.

In addition to the aforementioned techniques, transmit beamforming has also been extended to the aspect of time-division transmit beamforming [71] recently.

#### 2.1.3.3 Parameter estimation and Detection

There also have been abundant achievements for MIMO radar parameter estimation and detection [27, 74–88]. The earliest studies on these two issues have been reported in the literature [74] and [75] issued in the year of 2006. The work of [74] has focused on improving the detection performance by applying target spatial diversity to statistical MIMO radar. Effects caused by slow fluctuations of target reflection cross section have been fully studied in this work, and it has been shown that the optimal Neyman-Pearson-sense detector consists of noncoherent processing of the outputs at the receiver. The work of [75] has analyzed the performance of target detection, angular estimation accuracy, and angular resolution for MIMO radar. The generalized likelihood ratio test (GLRT) for target detection, maximum likelihood direction estimation as well as its CRB have been derived for an arbitrary signal coherence matrix in [75].

Some of the relevant research has focused on moving target parameter estimation and detection [27, 76, 85, 86]. The work of [76] has investigated the problem of moving target detection in the environment of Gaussian noise and clutter. GLRT detector has been established there. It has been shown that the (widely separated) MIMO radar approach is more suitable for handling moving targets with small radial velocities, especially for scenarios in which colocated array is unable to separate the target from the clutter. Other MIMO radar detections using GLTR have been considered in [85]

and [86]. It has been shown in both of the two works that constant false alarm rate can be achieved. The work of [27] has considered the parameter estimation problem for a moving target in noncoherent MIMO radar, in which an approach which makes use of the phase information associated with each transmit-receive path has been proposed.

There are also relevant works which have paid attentions to the joint parameter estimation and detection [77, 78], the sensitivity analysis of detection [84], and the detection in the presence of phase synchronization mismatch [83] or heterogeneous environment [80] for MIMO radar. In addition, the study of detection has also been extended to passive MIMO mode [87, 88].

#### 2.1.3.4 Interference suppression

The interference suppression related research in MIMO radar has also attracted a lot of interest [37, 41, 89–98]. This part of research covers the issues of GMTI [37, 89–91], STAP for clutter mitigation [41, 92, 93], rank estimation of clutter covariance matrix (with or without multipath) [92, 94, 95], and jammer suppression [92, 96, 97].

The main result that has been achieved about MIMO GMTI is that it enables potential improvements in clutter mitigation SINR loss and minimum detectable velocity for slow-moving targets. It has been shown that such improvements result from the extended aperture achieved in MIMO radar. By comparing to conventional single-input multiple-output approach, both theoretical and experimental research has been conducted to verify this in the past years.

The STAP techniques, which have been fully developed for PA radar during the past three decades, have also been introduced to MIMO radar. The main difference between MIMO radar STAP and PA radar STAP is that extra DOFs are introduced to the former because of the transmit waveform diversity. This has been shown to have two sides, i.e., more clutter subspace is allowed to be filtered out by the extra DOFs, however, the increase of the data dimension as well as the clutter/jammer rank makes MIMO STAP more complex [92]. The work of [92] has proposed a subspace STAP method in which the clutter subspace is computed using the geometry of the radar configuration rather than the received data. Prolate spheroidal wave function has been employed as the tool for the clutter subspace calculation. Using the calculated clutter subspace and also estimating the jammer-plus-noise subspace independently, the number of required data samples has been significantly reduced in [92]. The work of [93] has introduced the joint domain localized processing method [99] to MIMO radar. To reduce the number of required samples, the received spatial-temporal

data is transformed to angle-Doppler domain via joint transmit-receive beamforming techniques and discrete Fourier transformation, and localized angle-Doppler subdomain is selected for adaptive processing. The proposed clutter mitigation method in [93] has also presented an automatic stage-selective multistage Wiener filter algorithm to solve the corresponding adaptive processing problem.

The study on the rank of MIMO radar clutter covariance matrix has also been carried out. For example, the work of [92] has extended the clutter rank estimation rule of PA radar [36] to MIMO radar. It has been shown that the transmit waveform diversity in MIMO radar also contributes to the clutter rank, and the contributing extent is determined by the aperture ratio between the transmit and receive arrays. The work of [95] has analyzed the clutter rank in terms of waveform covariance matrix. Waveforms are not constrained to be orthogonal in this work, and hence it has been shown that the rank of MIMO radar clutter covariance matrix is related to both the rank and the structure of the waveform covariance matrix. The MIMO radar clutter rank estimation in the presence of multipath ground clutter has been studied in [94]. In this work, the transmit-receive directionality spectrum has been employed in estimating the multipath clutter rank.

The issue of jammer suppression has also been studied for MIMO radar by several works, and relevant research on this topic is still continuing. The suppression of jamming signal has been incorporated in the STAP method developed in [92], where the diagonal structure of the covariance matrix of jammers has been used to facilitate the STAP. The works of [96] and [97] have studied the problem of terrain-scattered jammer suppression by proposing beamspace techniques with reduced dimension and robust beamforming techniques. Spatial signature difference between the echoes from the target and jamming sources has been used in the proposed designs.

#### 2.1.3.5 Related experiments

Several experimental research on MIMO radar has been conducted by Lincoln Laboratory during the past years. For example, an experimental system operating at $L$ and $X$ bands had been established by the year of 2003 [100]. This reported experimental system is the earliest testbed (named MIMO multifunction digital array) which supports MIMO techniques. Another experiment [37] conducted in the year of 2009 is about airborne MIMO GMTI. It has been utilized to verify the potential of enhanced GMTI performance when using MIMO techniques.

#### 2.1.3.6 Current important research issues

Considerable amount of research with respect to MIMO radar is on its way, and more useful results starts to emerge nowadays. The new branches of MIMO radar research include MIMO compressive sensing [101,102], MIMO SAR [103,104], cognitive MIMO radar [55], etc.

## 2.2 Radar AF

The implication of radar AF is that it represents the time response of a filter matched to a given finite-energy signal when the signal is received with a time delay and a Doppler shift.

The radar AF originates from the theory of matched filter. For a certain matched filter, its impulse response is defined by a particular signal to which this filter is matched. The matching result means that maximum SNR can be achieved at the output of the filter. The matched-filter response to time-delayed and Doppler-shifted signal serves as the prototype of the radar AF.

### 2.2.1 Woodward's AF

The Woodward's AF, which has been used for the radar system with a single waveform (i.e., for PA radar configuration), is defined as [59]

$$|\chi(\tau, f_d)| \triangleq \left| \int_{-\infty}^{\infty} u(t) u^*(t+\tau) \exp\{j2\pi f_d t\} \mathrm{d}t \right| \tag{2.1}$$

where $\tau$ is the time delay, $f_d$ is the Doppler shift, and $u(t)$ is the complex envelop of a signal at time $t$. Positive time delay $\tau$ implies that the target is farther from the radar than the reference position ($\tau = 0$), and positive Doppler shift $f_d$ means that the target is moving towards the radar. Without loss of generality, the signal $u(t)$ is assumed to be a unit-energy signal, i.e.,

$$\int_{-\infty}^{\infty} |u(t)|^2 \mathrm{d}t = 1. \tag{2.2}$$

Some important properties of the Woodward's AF are as follows:

- Maximum value occurs at the origin

$$|\chi(\tau, f_d)| \leq |\chi(0,0)| = 1. \tag{2.3}$$

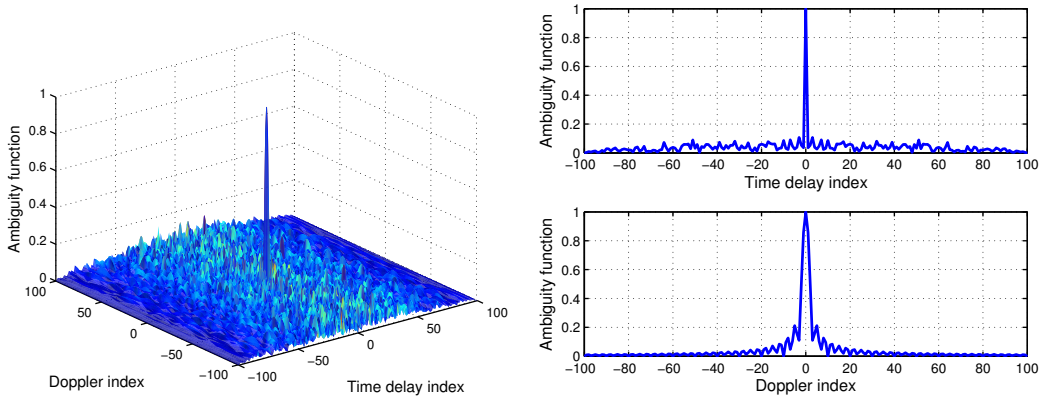


(a) (b)

Figure 2.1: The Woodward's AF and its zero-delay/Doppler cut for a single polyphase coded waveform.

- Constant volume

$$\int_{-\infty}^{\infty}\int_{-\infty}^{\infty}|\chi(\tau, f_d)|^2 \mathrm{d}\tau \mathrm{d}f_d = 1. \tag{2.4}$$

- Symmetry

$$|\chi(-\tau, -f_d)| = |\chi(\tau, f_d)|. \tag{2.5}$$

- Linear frequency modulation (LFM) effect, that is, if the complex envelope of the signal $u(t)$ has an AF $|\chi(\tau, f_d)|$, namely,

$$u(t) \Leftrightarrow |\chi(\tau, f_d)| \tag{2.6}$$

then the LFM signal $u(t)\exp\{j\pi kt^2\}$ leads to the AF $|\chi(\tau, f_d - k\tau)|$, i.e.,

$$u(t)\exp\{j\pi kt^2\} \Leftrightarrow |\chi(\tau, f_d - k\tau)|. \tag{2.7}$$

It is also interesting to see the zero-Doppler and zero-delay cuts of Woodward's AF, as shown in Figure 2.1 for an example, because the implications of both AF cuts are meaningful. Using (2.1), the zero-Doppler cut of the Woodward's AF can be expressed as

$$|\chi(\tau, 0)| = \left|\int_{-\infty}^{\infty} u(t)u^*(t+\tau)\mathrm{d}t\right| = |R(\tau)| \tag{2.8}$$

where $R(\tau)$ is the auto-correlation function of $u(t)$. This means that the zero-Doppler cut of Woodward's AF is the auto-correlation of the evaluated waveform. Similarly,

the zero-delay cut of Woodward's AF can be expressed as

$$|\chi(0, f_d)| = \left| \int_{-\infty}^{\infty} |u(t)|^2 e^{j2\pi f_d t} \mathrm{d}t \right| \tag{2.9}$$

which serves as the Fourier transform of the squared magnitude of the evaluated waveform $u(t)$.

### 2.2.2 MIMO radar AF

The Woodward's AF can not serve straightforwardly as MIMO radar AF simply because multiple waveforms are employed in MIMO radar. Therefore, particular AF should be defined for the MIMO radar configuration. Such defined MIMO radar AF is expected to serve as an efficient tool to characterize (local or global) resolution properties of the employed waveform set. This thesis deals with narrowband waveforms which are the most commonly used in radar field.

Among the existing works on MIMO radar, several definitions of MIMO radar AF exist. The work of [21] defines the MIMO radar AF as

$$\begin{aligned} \chi(\boldsymbol{\Theta}, \boldsymbol{\Theta}') \triangleq \Bigg| \sum_{n=1}^{N} \sum_{m'=1}^{M} \sum_{m=1}^{M} \int_{-\infty}^{\infty} & \phi_m(t - \tau_{m,n}(\mathbf{p})) \phi_{m'}^*(t - \tau_{m',n}(\mathbf{p}')) \\ & \times \exp\{-j2\pi\tau_{m,n}(\mathbf{p})(f_c + f_{m,n}(\boldsymbol{\Theta}))\} \exp\{j2\pi\tau_{m',n}(\mathbf{p}')(f_c + f_{m',n}(\boldsymbol{\Theta}'))\} \\ & \times \exp\{j2\pi(f_{m,n}(\boldsymbol{\Theta}) - f_{m',n}(\boldsymbol{\Theta}'))t\} \mathrm{d}t \Bigg|^2 \end{aligned} \tag{2.10}$$

where $M$ and $N$ are the numbers of transmit and receive antenna elements, respectively, $\phi_m(t - \tau_{m,n}(\mathbf{p}))$ and $\phi_{m'}(t - \tau_{m',n}(\mathbf{p}'))$ are the time-delayed versions of the $m$th and $m'$th transmitted waveforms $\phi_m(t)$ and $\phi_{m'}(t)$ with $\tau_{m,n}(\mathbf{p})$ and $\tau_{m',n}(\mathbf{p}')$ being the $(m, n)$th and $(m', n)$th transmit-receive path time delays associated with the target positions $\mathbf{p}$ and $\mathbf{p}'$, respectively, $f_{m,n}(\boldsymbol{\Theta})$ and $f_{m',n}(\boldsymbol{\Theta})$ are the $(m, n)$th and $(m', n)$th transmit-receive path Doppler frequencies associated with the target parameters $\boldsymbol{\Theta}$ and $\boldsymbol{\Theta}'$, respectively, $f_c$ is the carrier frequency, and $(\cdot)^*$ denotes the conjugate operation.

The second definition of MIMO radar AF can be found in the work of [23], which is expressed in the following form

$$|\chi(\tau, f_d)|^2 \triangleq \sum_{j=1}^{M} \sum_{k=1}^{M} |\chi_{jk}(\tau, f_d)|^2 \tag{2.11}$$

where

$$\chi_{jk}(\tau, f_d) \triangleq \int_{-\infty}^{\infty} \phi_j(t)\phi_k^*(t+\tau)e^{j2\pi f_d t}\mathrm{d}t \tag{2.12}$$

with $\phi_j(t)$ and $\phi_k(t)$ being the $j$th and $k$th transmitted waveforms of MIMO radar. We name this AF definition as square-summation-form MIMO radar AF.

Another version of MIMO radar AF, defined in [43], is similar to that of [21], hence it is not presented here. Note that there are also wide-band case MIMO radar AF (see [21]), however, this thesis focuses on the narrow-band case only. Thus, the wide-band MIMO radar AF is not presented.

# 3 Signal models and preliminaries

In this chapter, the signal model of the traditional MIMO radar is presented first. Then it is extended to the TB-based MIMO radar configuration. Preliminaries which include the existing TB matrix designs as well as their essence are presented in the latter part of this chapter.

## 3.1 Traditional MIMO radar signal model

Consider a colocated MIMO radar system with a transmit array of $M$ antenna elements and a receive array of $N$ antenna elements. Both the transmit and receive arrays are assumed to be closely located, therefore, they share an identical spatial angle for a far-field target. In the context of the traditional MIMO radar, the complex envelope of the waveforms emitted by the transmit antenna elements can be modeled as

$$s_m(\tilde{t}) = \sqrt{\frac{E}{M}}\phi_m(\tilde{t}),\ m = 1, 2, \ldots, M \tag{3.1}$$

where $E$ is the total transmit energy within one radar pulse, $\tilde{t}$ is the continuous fast-time index, i.e., time within the pulse, and $\phi_m(\tilde{t})$ is the $m$th orthogonal baseband waveform. Without loss of generality, we assume that the transmitted waveforms are normalized to have unit-energy, i.e.,

$$\int_T |\phi_m(\tilde{t})|^2 \mathrm{d}\tilde{t} = 1,\ m = 1, 2, \ldots, M \tag{3.2}$$

where $T$ is the time duration of the pulse.

Assuming that $L$ targets are present, the $N \times 1$ received complex signal vector can be expressed as

$$\mathbf{x}(t, \varsigma) = \sum_{l=1}^{L} r_l(t, \varsigma)\mathbf{b}(\theta_l) + \mathbf{z}(t, \varsigma) \tag{3.3}$$

where $t$ is the continuous fast-time index for the received signal, $\varsigma$ is the slow-time index, i.e., the pulse number, $\mathbf{b}(\theta_l)$ is the steering vector of the receive array associated with the $l$th target, $\mathbf{z}(t, \varsigma)$ is $N \times 1$ zero-mean white Gaussian noise, and

$$r_l(t, \varsigma) = \sqrt{\frac{E}{M}}\alpha_l(\varsigma)D_l(\varsigma)\mathbf{a}^T(\theta_l)\boldsymbol{\phi}(t) \tag{3.4}$$

is the echo of radar return due to the $l$th target located at the spatial direction $\theta_l$. In (3.4), $\alpha_l(\varsigma)$, $D_l(\varsigma)$, $\mathbf{a}(\theta_l)$, and $\theta_l$ are respectively the complex reflection coefficient

with variance $\sigma_\alpha^2$, the phase due to Doppler, the steering vector of transmit array, and the spatial angle all associated with the $l$th target, $\boldsymbol{\phi}(t) \triangleq [\phi_1(t), \ldots, \phi_M(t)]^T$ is the $M \times 1$ waveform vector, and $(\cdot)^T$ stands for the transpose operation. Note that the reflection coefficient $\alpha_l(\varsigma)$ is assumed to follow the Swerling II target model, i.e., it remains constant during the whole pulse, but varies independently from pulse to pulse. $D_l(\varsigma)$ is assumed to be constant for any give $t$ during the $\varsigma$th pulse, i.e., slow-moving targets are assumed.

At the receiving end, the $N \times 1$ component of the received data (3.4) due to the $m$th waveform is extracted by employing the matched filtering technique, i.e.,

$$\mathbf{x}_m(\varsigma) \triangleq \int_T \mathbf{x}(t, \varsigma)\phi_m^*(t)\mathrm{d}t, \ m = 1, \ldots, M \tag{3.5}$$

where $(\cdot)^*$ is the conjugate operator. By stacking all the filtered components (3.5) into a column vector, we can obtain the following $MN \times 1$ virtual data vector

$$\begin{aligned} \mathbf{y}_{\mathrm{MIMO}}(\varsigma) &\triangleq \left[\mathbf{x}_1^T(\varsigma), \ldots, \mathbf{x}_M^T(\varsigma)\right]^T \\ &= \sqrt{\frac{E}{M}} \sum_{l=1}^{L} \alpha_l(\varsigma) D_l(\varsigma) \mathbf{u}_{\mathrm{MIMO}}(\theta_l) + \tilde{\mathbf{z}}(\varsigma) \end{aligned} \tag{3.6}$$

where $\mathbf{u}_{\mathrm{MIMO}} \triangleq \mathbf{a}(\theta) \otimes \mathbf{b}(\theta)$ is the $MN \times 1$ virtual steering vector, $\tilde{\mathbf{z}}(\varsigma)$ is the $MN \times 1$ noise term whose covariance is given by $\sigma_{\mathbf{z}}^2 \mathbf{I}_{MN}$, and $\otimes$ denotes the Kronecker product.

## 3.2 TB-based MIMO radar signal model

Different from the traditional MIMO radar that emits waveforms omni-directionally, the TB-based MIMO radar aims at focusing the energy of multiple transmitted waveforms within a spatial sector-of-interest $\boldsymbol{\Omega}$ via a certain number of beams. The sector $\boldsymbol{\Omega}$ can be estimated in a preprocessing stage of low-resolution DOA estimation with low complexity.

In the TB-based MIMO radar system, $K$ (in general, $K \leq M$) initially orthogonal waveforms are transmitted [8]. For each waveform, a transmit beam that illuminates a certain area within the pre-determined spatial angular sector-of-interest $\boldsymbol{\Omega}$ is formed. The $K$ synthesized transmit beams are designed to fully cover the spatial sector $\boldsymbol{\Omega}$. Thus, in the context of the TB-based MIMO radar, the signal radiated towards the target located at the spatial direction $\theta$ via the $k$th transmit beam can be modeled

as [8]

$$s_k(t) = \sqrt{\frac{E}{K}}\mathbf{c}_k^T\mathbf{a}(\theta)\phi_k(t),\ k = 1, \ldots, K \tag{3.7}$$

where $\mathbf{c}_k$ is the $k$th column vector of the $M \times K$ TB matrix $\mathbf{C}$ with $\mathbf{C}$ being defined as

$$\mathbf{C} \triangleq [\mathbf{c}_1, \ldots, \mathbf{c}_K]. \tag{3.8}$$

Technically, each column of $\mathbf{C}$ that is composed of $M$ elements is elaborately designed to form a certain transmit beam within the sector-of-interest $\mathbf{\Omega}$, and the $k$th orthogonal waveform is emitted through the $k$th synthesized transmit beam. Therefore, by denoting the $m$th element of $\mathbf{c}_k$ as $c_{mk}$, the signal $\tilde{s}_m(t)$ radiated from the $m$th transmit antenna element can be expressed as

$$\tilde{s}_m(t) = \sqrt{\frac{E}{K}}\sum_{k=1}^{K} c_{mk}\phi_k(t),\ m = 1, \ldots, M. \tag{3.9}$$

The signal model (3.9) servers as the foundation of the TB-based MIMO radar AF defined in the following chapter. To make it complete, the whole signal processing model of the TB-based MIMO radar is presented here.

At the receiving end, the $N \times 1$ complex vector of array observations can be expressed as

$$\mathbf{x}_{\text{beam}}(t, \varsigma) = \sum_{l=1}^{L} \tilde{r}_l(t, \varsigma)\mathbf{b}(\theta_l) + \mathbf{z}(t, \varsigma) \tag{3.10}$$

where

$$\tilde{r}_l(t, \varsigma) = \sqrt{\frac{E}{M}}\alpha_l(\varsigma)D_l(\varsigma)\Big(\mathbf{C}^T\mathbf{a}(\theta_l)\Big)^T\boldsymbol{\phi}(t) \tag{3.11}$$

and other variables as well as parameters are the same as that in the traditional MIMO radar signal model part.

By matched filtering $\mathbf{x}_{\text{beam}}(t, \varsigma)$ to each of the original orthogonal waveforms $\phi_k(t), k = 1, \ldots, K$, the received signal component associated with each of the transmitted waveforms can be expressed as

$$\begin{aligned}\mathbf{x}_{\text{beam},k}(\varsigma) &\triangleq \int_T \mathbf{x}_{\text{beam}}(t, \varsigma)\phi_k^*(t)\mathrm{d}t \\ &= \sqrt{\frac{E}{M}}\sum_{l=1}^{L}\alpha_l(\varsigma)D_l(\varsigma)\Big(\mathbf{c}_k^T\mathbf{a}(\theta_l)\Big)\mathbf{b}(\theta_l) + \bar{\mathbf{z}}_k(t, \varsigma)\end{aligned} \tag{3.12}$$

where the $N \times 1$ noise term can be expressed as

$$\bar{\mathbf{z}}_k(t,\varsigma) \triangleq \int_T \mathbf{z}(t,\varsigma)\phi_k^*(t)\mathrm{d}t. \tag{3.13}$$

By stacking all the $K$ match-filtered components (3.12) into one column vector, the $KN \times 1$ virtual data vector $\mathbf{y}_{\text{beam}}$ can be obtained as

$$\begin{aligned}\mathbf{y}_{\text{TB}}(\varsigma) &\triangleq \left[\mathbf{x}_{\text{beam},1}^T(\varsigma),\ldots,\mathbf{x}_{\text{beam},K}^T(\varsigma)\right]^T \\ &= \sqrt{\frac{E}{M}}\sum_{l=1}^{L}\alpha_l(\varsigma)D_l(\varsigma)\mathbf{u}_{\text{TB}}(\theta_l)+\bar{\mathbf{z}}(\varsigma)\end{aligned} \tag{3.14}$$

where $\mathbf{u}_{\text{TB}} \triangleq (\mathbf{C}^T\mathbf{a}(\theta)) \otimes \mathbf{b}(\theta)$ is the $KN \times 1$ virtual steering vector of the TB-based MIMO radar and $\bar{\mathbf{z}}(\varsigma) \triangleq [\bar{\mathbf{z}}_1(\varsigma),\ldots,\bar{\mathbf{z}}_K(\varsigma)]^T$ is the $KN \times 1$ noise term whose covariance is given by $\sigma_{\mathbf{z}}^2\mathbf{I}_{KN}$.

## 3.3 Preliminaries of TB designs

Some TB design strategies have been developed in the past few years [8,9,12,15,105], and the way of designing the TB matrix $\mathbf{C}$ depends on the objective of radar designer. For example, desired beampattern (possibly flat) or perfect phase rotations among synthesized beams for DOA estimation may be required. In the following, we present the spheroidal sequences-based and the convex optimization-based methods [8] as two examples. The former ensures to achieve perfect beampattern, while the latter aims at approximating desired (possibly linear) phase rotations.

### 3.3.1 Spheroidal sequences-based design

The spheroidal sequences-based method aims at maximizing the ratio between the energy radiated within the desired spatial sector $\mathbf{\Omega}$ and the total transmit energy for each of the synthesized transmit beams. For the $k$th ($k \in \{1,\ldots,K\}$) transmit beam, it can be formulated as the following optimization problem [8]

$$\max_{\mathbf{c}_k} \quad \frac{\mathbf{c}_k^H\mathbf{A}\mathbf{c}_k}{\int_{-\frac{\pi}{2}}^{\frac{\pi}{2}}|\mathbf{c}_k^H\mathbf{a}(\theta)|^2\mathrm{d}\theta} \tag{3.15}$$

where the nonnegative matrix $\mathbf{A}$ is defined as

$$\mathbf{A} \triangleq \int_{\mathbf{\Omega}} \mathbf{a}(\theta)\mathbf{a}^H(\theta)\mathrm{d}\theta. \tag{3.16}$$

The solution to this method is found to be composed of the $K$ eigenvectors of the matrix $\mathbf{A}$, corresponding to its $K$ largest eigenvalues, i.e.,

$$\mathbf{C} = [\mathbf{v}_1, \ldots, \mathbf{v}_K] \tag{3.17}$$

where $\{\mathbf{v}_k\}_{k=1}^K$ are the $K$ principal eigenvectors of the negative matrix $\mathbf{A}$. This means that the number of transmitted waveforms in the TB-based MIMO radar is taken as the number of effective eigenvalues of the matrix $\mathbf{A}$. This effectiveness is guaranteed by enabling the sum of the $K$ largest corresponding eigenvalues to exceed a certain percentage (e.g., 99%) of the total sum of all eigenvalues of $\mathbf{A}$.

It is worth noting that this nonadaptive method can be used as the foundation for other derived TB designs that require good beampattern while achieving other goals at the same time. For example, the TB matrix $\mathbf{C}$ in (3.17) can be used as a quiescent beamspace matrix for jammer suppression [96].

### 3.3.2 Convex optimization-based design

The convex optimization-based design, which employs convex optimization techniques, formulates the TB design as a certain type of convex optimization problem such as second-order cone programming (SOCP) or semi-definite programming (SDP) [57] problem. The presented convex optimization-based TB strategy is obtained in the form of an SOCP optimization problem. The objective is to minimize the largest difference between the designed and the desired phase rotations among the synthesized transmit beams with their directions towards the sector-of-interest $\mathbf{\Omega}$, while minimizing (or keeping fixed) the energy transmitted in the out-of-sector area $\bar{\mathbf{\Omega}}$ at the same time [8]. Mathematically, the constrained optimization problem for finding the corresponding TB matrix $\mathbf{C}$ can be expressed as

$$\begin{aligned} \min_{\mathbf{C}} \max_{i} \quad & \left\| \mathbf{C}^H\mathbf{a}(\theta_i) - \mathbf{d}(\theta_i) \right\|, \ \theta_i \in \mathbf{\Omega}, \ i = 1, \ldots, I \\ \text{s.t.} \quad & \left\| \mathbf{C}^H\mathbf{a}(\theta_j) \right\| \leq \gamma, \qquad \bar{\theta}_j \in \bar{\mathbf{\Omega}}, \ j = 1, \ldots, J \end{aligned} \tag{3.18}$$

where $\mathbf{d}(\theta)$ is the presumed vector of size $K \times 1$ that guarantees the desired phase rotation property of transmit beamforming, $\bar{\mathbf{\Omega}}$ combines a continuum of all out-

of-sector directions that lie outside $\mathbf{\Omega}$, $\gamma$ is the parameter of the user choice that characterizes the worst acceptable level of transmit power leakage in the out-of-sector region, $I$ and $J$ are the numbers of grids of angles within and outside the sector-of-interest $\mathbf{\Omega}$, respectively, and $\|\cdot\|$ is the Euclidean norm. Note that other TB methods using convex optimization techniques can also be proposed, if proper objective function and constraints are elaborated.

### 3.3.3 Essence of TB designs

The correlated waveforms $\mathbf{S}(t) \triangleq [\tilde{s}_1(t), \ldots, \tilde{s}_M(t)]$ can also be designed directly [105]. To achieve good Doppler tolerance of the waveforms, spectral constraints can be enforced in the designing process [106]. In essence, both the TB matrix design and the direct correlated waveforms design can be understood as achieving an optimal (in some predetermined sense) covariance matrix $\mathbf{R}_{\mathrm{d}}$ that can be expressed as $\mathbf{R}_{\mathrm{d}} = \mathbf{C}\mathbf{C}^H$ or as $\mathbf{R}_{\mathrm{d}} = \mathbb{E}\{\mathbf{S}(t)\mathbf{S}^H(t)\}$ with $\mathbb{E}\{\cdot\}$ standing for the expectation operator. In contrast to designing the covariance matrix $\mathbf{R}_{\mathrm{d}}$ directly [9], the TB-based approach enables us to define and investigate the AF of the TB-based MIMO radar.

# 4 The TB-based MIMO radar AF

In this chapter, we first introduce the AF of the TB-based MIMO radar, then we establish the relationships among the so-defined AF and the previous works on AF including the well-known Woodward's AF, the traditional MIMO radar AF, and the PA radar AF.

## 4.1 AF Definition and Implication

### 4.1.1 Definition

We consider the most common radar scenario of far-field targets and narrow-band waveforms, and assume that the TB-based MIMO radar is operating at the frequency $f_c$. For a point target located at the position $\mathbf{p}$, the received signal at the $j$th receive antenna element before demodulation to the base band can be written as

$$\tilde{r}_j(t,\mathbf{p}) = \sum_{m=1}^{M} \alpha_{mj}\tilde{s}_m(t-\tau_{mj}(\mathbf{p})) \times \exp\{j2\pi f_c(t-\tau_{mj}(\mathbf{p}))\} + \tilde{z}_j(t) \tag{4.1}$$

where $\alpha_{mj}$ is the complex reflection coefficient for the $(m,j)$th transmit-receive channel, $\tau_{mj}(\mathbf{p})$ is the two-way time delay of the $(m,j)$th transmit-receive channel due to the target location at $\mathbf{p}$, $\tilde{s}_m(t-\tau_{mj}(\mathbf{p}))$ is the time-delayed version of $\tilde{s}_m(t)$ that has been defined in (3.9), and $\tilde{z}_j(t)$ is the noise observed by the $j$th receive antenna element.

Let us assume that the target is moving, and its velocity and moving direction are depicted by the vector $\mathbf{v}$. For the sake of brevity, we exploit $\mathbf{\Theta}$ to denote the parameter of a variable in the following derivation if it is determined by both the target position $\mathbf{p}$ and the velocity vector $\mathbf{v}$. Considering the effect of target motion on Doppler in (4.1) and using also (3.9), the received signal after performing demodulation to the baseband can be expressed as

$$\hat{r}_j(t,\mathbf{\Theta}) = \sqrt{\frac{E}{K}} \sum_{m=1}^{M}\sum_{k=1}^{K} \alpha_{mj}c_{mk}\phi_k(t-\tau_{mj}(\mathbf{p}))\exp\{-j2\pi\tau_{mj}(\mathbf{p})(f_c+f_{mj}(\mathbf{\Theta}))\} \times \exp\{j2\pi f_{mj}(\mathbf{\Theta})t\} + z_j(t) \tag{4.2}$$

where $f_{mj}(\mathbf{\Theta})$ is the Doppler shift of the target due to the $(m,j)$th transmit-receive channel and $z_j(t)$ is the white Gaussian noise with power $\sigma_z^2$ observed at the $j$th

receive antenna element after demodulation.

At the receiving end, a bank of matched filters is employed due to the fact that the received signal is a sum of the reflected echoes associated with the known transmitted waveforms. The optimal detector is a filter matched to a specific set of target parameters. Therefore, by matched filtering $\hat{r}_j(t,\boldsymbol{\Theta})$ to each of the waveforms $\phi_k(t)$, $k=1,\ldots,K$ with a specific target parameter $\boldsymbol{\Theta}'$, namely, $\phi_k(t,\boldsymbol{\Theta}')$, $k=1,\ldots,K$, the received signal component associated with the $i$th transmitted waveform can be obtained as

$$\begin{aligned}\bar{r}_{ji}(\boldsymbol{\Theta},\boldsymbol{\Theta}') &= \int \hat{r}_j(t,\boldsymbol{\Theta})\phi_i^*(t,\boldsymbol{\Theta}')\mathrm{d}t \\ &= \sqrt{\frac{E}{K}}\sum_{m=1}^{M}\sum_{k=1}^{K}\alpha_{mj}\int c_{mk}\phi_k(t-\tau_{mj}(\mathbf{p}))\phi_i^*(t-\tau_{q(i)j}(\mathbf{p}'))\exp\{-j2\pi\tau_{mj}(\mathbf{p}) \\ &\quad \times (f_c+f_{mj}(\boldsymbol{\Theta}))\}\exp\{j2\pi\tau_{q(i)j}(\mathbf{p}')(f_c+f_{q(i)j}(\boldsymbol{\Theta}'))\} \\ &\quad \times \exp\{j2\pi(f_{mj}(\boldsymbol{\Theta})-f_{q(i)j}(\boldsymbol{\Theta}'))t\}\mathrm{d}t+\bar{z}_{ji}(t) \\ &\triangleq \bar{r}'_{ji}(\boldsymbol{\Theta},\boldsymbol{\Theta}')+\bar{z}_{ji}(t) \end{aligned} \tag{4.3}$$

where $q(i)$ is the equivalent transmit phase center for the $i$th transmitted waveform and $\bar{z}_{ji}(t)$ is the noise after matched filtering.

Let us define the AF as the square of coherent summation of all the noise-free matched filtering output pairs $(j,i)$, $j=1,\ldots,N$ and $i=1,\ldots,K$. Thus, the AF of the TB-based MIMO radar can be mathematically expressed as

$$\begin{aligned}\chi(\boldsymbol{\Theta},\boldsymbol{\Theta}') &\triangleq \left|\sum_{j=1}^{N}\sum_{i=1}^{K}\bar{r}'_{ji}(\boldsymbol{\Theta},\boldsymbol{\Theta}')\right|^2 \\ &= \left|\sqrt{\frac{E}{K}}\sum_{j=1}^{N}\sum_{i=1}^{K}\sum_{m=1}^{M}\sum_{k=1}^{K}\alpha_{mj}\int c_{mk}\phi_k(t-\tau_{mj}(\mathbf{p}))\phi_i^*(t-\tau_{q(i)j}(\mathbf{p}')) \right. \\ &\quad \times \exp\{-j2\pi\tau_{mj}(\mathbf{p})(f_c+f_{mj}(\boldsymbol{\Theta}))\}\exp\{j2\pi\tau_{q(i)j}(\mathbf{p}')(f_c+f_{q(i)j}(\boldsymbol{\Theta}'))\} \\ &\quad \left.\times \exp\{j2\pi(f_{mj}(\boldsymbol{\Theta})-f_{q(i)j}(\boldsymbol{\Theta}'))t\}\mathrm{d}t\right|^2. \end{aligned} \tag{4.4}$$

Introducing an $M\times K$ matrix $\mathbf{R}$ whose $(m,i)$th element is defined as

$$\begin{aligned}[\mathbf{R}]_{mi}(\boldsymbol{\Theta},\boldsymbol{\Theta}',\mathbf{C},j) &\triangleq \sqrt{\frac{E}{K}}\sum_{k=1}^{K}c_{mk}\int \phi_k(t-\tau_{mj}(\mathbf{p}))\phi_i^*(t-\tau_{q(i)j}(\mathbf{p}')) \\ &\quad \times \exp\{j2\pi(f_{mj}(\boldsymbol{\Theta})-f_{q(i)j}(\boldsymbol{\Theta}'))t\}\mathrm{d}t \end{aligned} \tag{4.5}$$

the TB-based MIMO radar AF (4.4) can be simplified as

$$\chi(\boldsymbol{\Theta},\boldsymbol{\Theta}') = \left| \sum_{j=1}^{N}\sum_{i=1}^{K}\sum_{m=1}^{M} \alpha_{mj}[\mathbf{R}]_{mi}(\boldsymbol{\Theta},\boldsymbol{\Theta}',\mathbf{C},j)\exp\{-j2\pi\tau_{mj}(\mathbf{p})(f_c+f_{mj}(\boldsymbol{\Theta}))\} \right.$$
$$\left. \times \exp\{j2\pi\tau_{q(i)j}(\mathbf{p}')(f_c+f_{q(i)j}(\boldsymbol{\Theta}'))\} \right|^2 . \tag{4.6}$$

### 4.1.2 Implication

The TB-based MIMO radar AF (4.6) is composed of square of summation terms, and each summation term contains two more components in addition to the complex reflection coefficient part. One is the match-filtered component denoted by the matrix $\mathbf{R}$ that has been expressed by (4.5), which stands for the effect of waveform properties, i.e., the auto- and cross-correlations of the transmitted waveforms, and their Doppler tolerance. The other component is composed of the last two exponential terms in (4.6), and it stands for the phase shift information due to the relative target position and motion with respect to the transmit and receive arrays. The TB-based MIMO radar AF (4.6) can also be understood as follows. The $m$th transmit antenna element emits a compound signal that contains all the $K$ orthogonal waveforms, and these waveforms are windowed by the elements of the $m$th row in the TB matrix $\mathbf{C}$. Consequently, the matrix $\mathbf{R}$ should be of size $M \times K$, meaning that the TB matrix $\mathbf{C}$ has been employed to transform the original $K \times K$ matrix of waveform properties to $\mathbf{R}$. This presents the most significant difference that distinguishes the TB-based MIMO radar AF from the traditional MIMO radar AF. Therefore, the AF defined in [21] is not applicable to the TB-based MIMO radar.

The main objective of incorporating phase shift information in (4.6) is for taking into account the property of coherent processing introduced by the colocated array geometry and the specific radar configuration. Therefore, if the $i$th equivalent transmit phase center is selected to be the position of the $i$th transmit antenna element, it matches the way of processing in the traditional MIMO radar. If the position of the first (or the reference) transmit antenna element is selected, then it matches the case in the PA radar. The equivalent transmit phase centers of the TB-based MIMO radar depend on the exact form of the TB matrix $\mathbf{C}$. By properly designing the matrix $\mathbf{C}$ and the equivalent transmit phase centers, the AF (4.6) can serve as the AF of the PA, the traditional MIMO, and the TB-based MIMO radars. Hence, it can be viewed as a generalized AF form for the currently existing radar configurations.

## 4.2 Simplification and relationships with other AFs

### 4.2.1 AF simplification

The standard assumption of far-field targets and narrow-band waveforms is used in this thesis. The antenna elements of the transmit and receive arrays have locations $\{\mathbf{q}_{\mathrm{T},1},\ldots,\mathbf{q}_{\mathrm{T},M}\}$ and $\{\mathbf{q}_{\mathrm{R},1},\ldots,\mathbf{q}_{\mathrm{R},N}\}$ in three-dimensional Cartesian coordinate system, respectively. The equivalent transmit phase centers are assumed to have locations $\{\mathbf{q}_{\mathrm{TE},1},\ldots,\mathbf{q}_{\mathrm{TE},K}\}$. Here $\mathbf{q}_{\mathrm{T},i}$, $i=1,\ldots,M$; $\mathbf{q}_{\mathrm{R},i}$, $i=1,\ldots,N$; and $\mathbf{q}_{\mathrm{TE},i}$, $i=1,\ldots,K$ are all $1\times 3$ vectors. In addition, we let $\mathbf{u}(\boldsymbol{\Theta})$ be a unit-norm direction vector pointing from the transmit/receive array to the target identified by the parameter $\boldsymbol{\Theta}$.

We can neglect the effect of target reflection coefficients for different transmit-receive channels, i.e., assume that all $\alpha_{mj}$ are equal to one. This assumption is valid because the contributions of transmit-receive channels to the TB-based MIMO radar AF are constant at any given time $t$ under the standard case of far-field targets and narrow-band waveforms. The effect of $\alpha_{mj}$ on the TB-based MIMO radar AF is still constant even when considering multiple pulses and inter-pulse varying target reflection coefficients if wide pulse is employed and no range foldering [22] occurs. Then the AF (4.6) can be simplified as

$$\chi(\boldsymbol{\Theta},\boldsymbol{\Theta}')=\left|\mathbf{a}_{\mathrm{R}}^{H}(\boldsymbol{\Theta})\mathbf{a}_{\mathrm{R}}(\boldsymbol{\Theta}')\right|^{2}\left|\mathbf{a}_{\mathrm{T}}^{H}(\boldsymbol{\Theta})\bar{\mathbf{R}}\mathbf{a}_{\mathrm{TE}}(\boldsymbol{\Theta}')\right|^{2} \tag{4.7}$$

where the $(m,i)$th element of the $M\times K$ matrix $\bar{\mathbf{R}}$ is expressed as

$$\left[\bar{\mathbf{R}}\right]_{mi}(\Delta\tau,\Delta f_d,\mathbf{C})=\sqrt{\frac{E}{K}}\sum_{k=1}^{K}c_{mk}\int\phi_k(t)\phi_i^{*}(t-\Delta\tau)\exp\{j2\pi\Delta f_d t\}\mathrm{d}t \tag{4.8}$$

and $(\cdot)^H$ denotes the conjugate transpose. Here also $\Delta\tau\triangleq\tau(\mathbf{p})-\tau(\mathbf{p}')$, $\Delta f_d\triangleq f(\boldsymbol{\Theta})-f(\boldsymbol{\Theta}')$, and

$$\mathbf{a}_{\mathrm{T}}(\boldsymbol{\Theta})\triangleq\left[\exp\left\{\tilde{\mathbf{u}}^{T}(\boldsymbol{\Theta})\mathbf{q}_{\mathrm{T},1}\right\},\ldots,\exp\left\{\tilde{\mathbf{u}}^{T}(\boldsymbol{\Theta})\mathbf{q}_{\mathrm{T},M}\right\}\right]^{T} \tag{4.9}$$

$$\mathbf{a}_{\mathrm{R}}(\boldsymbol{\Theta})\triangleq\left[\exp\left\{\tilde{\mathbf{u}}^{T}(\boldsymbol{\Theta})\mathbf{q}_{\mathrm{R},1}\right\},\ldots,\exp\left\{\tilde{\mathbf{u}}^{T}(\boldsymbol{\Theta})\mathbf{q}_{\mathrm{R},N}\right\}\right]^{T} \tag{4.10}$$

$$\mathbf{a}_{\mathrm{TE}}(\boldsymbol{\Theta})\triangleq\left[\exp\left\{\tilde{\mathbf{u}}^{T}(\boldsymbol{\Theta})\mathbf{q}_{\mathrm{TE},1}\right\},\ldots,\exp\left\{\tilde{\mathbf{u}}^{T}(\boldsymbol{\Theta})\mathbf{q}_{\mathrm{TE},K}\right\}\right]^{T} \tag{4.11}$$

are the $M\times 1$ transmit steering vector, the $N\times 1$ receive steering vector, and the $K\times 1$ equivalent transmit steering vector, respectively, with $\tilde{\mathbf{u}}(\boldsymbol{\Theta})\triangleq j2\pi f'(\boldsymbol{\Theta})\cdot\mathbf{u}(\boldsymbol{\Theta})/c$

and $f'(\boldsymbol{\Theta}) \triangleq f_c + f(\boldsymbol{\Theta})$. The dependence of $\bar{\mathbf{R}}$ from $\Delta\tau, \Delta f_d$, and $\mathbf{C}$ is not shown in (4.7) for brevity, and the subscript indices for $\tau$ and $f$ are omitted since we consider the case of far-field target and narrow-band waveforms.

It is known that the Woodward's AF for a single waveform $u(t)$ can be expressed as

$$\bar{\chi}(\tau, f_d) = \int u(t)u^*(t-\tau)\exp\{j2\pi f_d t\}\mathrm{d}t. \tag{4.12}$$

Based on this expression, we can define the $K \times K$ matrix $\bar{\boldsymbol{\chi}}(\tau, f_d)$ as the AF matrix of the $K$ orthogonal waveforms for the TB-based MIMO radar. The $(j,k)$th element of $\bar{\boldsymbol{\chi}}(\tau, f_d)$ is given by

$$[\bar{\boldsymbol{\chi}}]_{jk}(\tau, f_d) = \int \phi_j(t)\phi_k^*(t-\tau)\exp\{j2\pi f_d t\}\mathrm{d}t. \tag{4.13}$$

Using (4.8) and (4.13), the AF (4.7) can be expressed as

$$\chi(\boldsymbol{\Theta}, \boldsymbol{\Theta}') = \frac{E}{K}\left|\mathbf{a}_{\mathrm{R}}^H(\boldsymbol{\Theta})\mathbf{a}_{\mathrm{R}}(\boldsymbol{\Theta}')\right|^2 \left|\mathbf{a}_{\mathrm{T}}^H(\boldsymbol{\Theta})\mathbf{C}\bar{\boldsymbol{\chi}}(\Delta\tau, \Delta f_d)\mathbf{a}_{\mathrm{TE}}(\boldsymbol{\Theta}')\right|^2 \tag{4.14}$$

where $\bar{\boldsymbol{\chi}}(\Delta\tau, \Delta f_d)$ is the $K \times K$ matrix whose elements are obtained from (4.13) by changing the parameters $\tau$ and $f_d$ into $\Delta\tau$ and $\Delta f_d$, respectively. Realizing that $\Delta\tau$ and $\Delta f_d$ depend on $\boldsymbol{\Theta}$ and $\boldsymbol{\Theta}'$, we employ these two parameters to denote the TB-based MIMO radar AF. In the following, we show how the derived AF is a generalization of the widely used AF results for different radar configurations.

### 4.2.2 Relationship with Woodward's AF

Equation (4.14) establishes the connection between the TB-based MIMO radar AF and the well known Woodward's AF. The TB matrix $\mathbf{C}$ transforms the original transmit steering vector of length $M$ into a new one of length $K$. Both the transformed and the equivalent transmit steering vectors are acting on the $K$ waveforms' Woodward AF matrix, representing both the coherent transmit processing gain and the waveform diversity. Equivalently, we can say that each AF is windowed by the product of a coherent processing gain and an equivalent transmit phase term. To be precise, for the $j$th and $k$th waveforms, the quantity $[\bar{\boldsymbol{\chi}}(\Delta\tau, \Delta f_d)]_{jk}$, $j, k \in \{1, \ldots, K\}$ is windowed by the product of the $j$th coherent processing gain, namely, $\Upsilon_j \triangleq \mathbf{a}_{\mathrm{T}}^H(\boldsymbol{\Theta})\mathbf{c}_j$ and the $k$th equivalent transmit phase term which is denoted by the $k$th element of $\mathbf{a}_{\mathrm{TE}}(\boldsymbol{\Theta}')$.

### 4.2.3 Relationship with the traditional MIMO radar AF

Equation (4.14) establishes the connection between the TB-based MIMO radar AF and the traditional MIMO radar AF. If the number of transmitted waveforms $K$ is increased to $M$, $\mathbf{C}$ is simply the $M \times M$ identity matrix $\mathbf{I}_M$, and the equivalent transmit phase centers are selected to be the positions of the $M$ individual transmit antenna elements, then the TB-based MIMO radar AF (4.14) becomes the following form

$$\chi_{\mathrm{MIMO}}(\boldsymbol{\Theta}, \boldsymbol{\Theta}') = \frac{E}{M}\left|\mathbf{a}_{\mathrm{R}}^{H}(\boldsymbol{\Theta})\mathbf{a}_{\mathrm{R}}(\boldsymbol{\Theta}')\right|^{2}\left|\mathbf{a}_{\mathrm{T}}^{H}(\boldsymbol{\Theta})\bar{\boldsymbol{\chi}}(\Delta\tau, \Delta f_d)\mathbf{a}_{\mathrm{T}}(\boldsymbol{\Theta}')\right|^{2} \tag{4.15}$$

which denotes the traditional MIMO radar AF and has exactly the same form as the AF definition in [21] except for the magnitude term. This term represents the general expression of the transmit power allocation for the traditional MIMO radar. Therefore, if $E$ is selected to be equal to $M$, the expression (4.15) and the definition of AF in [21] have identical expressions. Furthermore, the TB-based MIMO radar AF (4.14) also shows compatibility with the traditional MIMO radar with $K$ uniform subarrays [7], if $\mathbf{C}$ is properly designed to be a block diagonal TB matrix whose block diagonal elements are associated with the subarrays. The equivalent phase centers in this case are selected as the centers of subarrays.

### 4.2.4 Relationship with the PA radar AF

Equation (4.14) also establishes the connection between the TB-based MIMO radar AF and the PA radar AF. If the number of transmitted waveforms $K$ is decreased to 1, $\mathbf{C}$ becomes just a beamforming weight vector $\mathbf{w}$, and the equivalent transmit phase center is selected to be the first (or the reference) transmit antenna. Then the TB-based MIMO radar AF takes the following form

$$\chi_{\mathrm{PA}}(\boldsymbol{\Theta}, \boldsymbol{\Theta}') = E\left|\mathbf{a}_{\mathrm{R}}^{H}(\boldsymbol{\Theta})\mathbf{a}_{\mathrm{R}}(\boldsymbol{\Theta}')\right|^{2}\left|\mathbf{a}_{\mathrm{T}}^{H}(\boldsymbol{\Theta})\mathbf{w}\bar{\chi}(\Delta\tau, \Delta f_d)\right|^{2} \tag{4.16}$$

where $\bar{\chi}(\Delta\tau, \Delta f_d)$ is the Woodward's AF for the only transmitted waveform in PA radar. Equation (4.16) is also obtained from (4.13) by changing the parameters $\tau$ and $f_d$ into $\Delta\tau$ and $\Delta f_d$, respectively. Considering that the magnitude of the equivalent transmit phase center in the PA mode is constant, it can be neglected when deriving (4.16). Consequently, the TB-based MIMO radar AF defined in this thesis serves as a universal AF definition for the traditional MIMO radar (with subarrays) and the PA radar. Moreover, this generalized AF definition can be expressed using the

Woodward's AF matrix which links it to the Woodward's AF.

Compared to the traditional MIMO radar AF in [23] which defines it as the sum of squared noise-free match-filtered outputs, the TB-based MIMO radar AF (4.14) incorporates phase shift information introduced by the array geometry and the relative motion, and furthermore exploits the square of summation of all the auto- and cross-AF terms of the $K$ waveforms as the TB-based MIMO radar AF metric. This operation enables it to obtain lower-level relative sidelobes in the Doppler-delay domain than that of the AF in [23]. The reason lies in the mathematical expression itself and the waveform orthogonality. Moreover, the TB-based MIMO radar AF (4.14) conforms to the practically known fact that all the matched filtering outputs for each pair of two different waveforms are mixed together at the receiving end. Thus, the TB-based MIMO radar AF (4.14) is a more practical and suitable AF metric. On the other hand, the existing AF definitions in [21] and [23] for the traditional MIMO radar and the AF defined here for the TB-based MIMO radar are all based on the Woodward's AF.

## 4.3 New TB design

The existing TB strategies are designed based on zero-Doppler and zero-delay AF cut, i.e., only spatial information is incorporated in the designs. Therefore, we can also control the relative sidelobe levels of the TB-based MIMO radar AF by enforcing additional constraints on different Doppler and delay bins during the design process of the TB matrix $\mathbf{C}$. For example, if the relative sidelobes of the TB-based MIMO radar AF within certain Doppler and delay sectors-of-interest $\mathfrak{F}$ and $\mathfrak{D}$ are desired to be kept below a certain level, the TB strategy (3.18) can be redesigned by solving the following optimization problem

$$\min_{\mathbf{C}} \max_{i} \ \left\|\mathbf{C}^H\mathbf{a}_{\mathrm{T}}(\boldsymbol{\theta}_i)\odot\mathbf{a}_{\mathrm{TE}}(\boldsymbol{\theta}_i)-\mathbf{d}(\boldsymbol{\theta}_i)\right\|,\ \boldsymbol{\theta}_i\in\boldsymbol{\Omega},\ i=1,\ldots,I \tag{4.17a}$$

$$\text{s.t.} \quad \left\|\mathbf{C}^H\mathbf{a}_{\mathrm{T}}(\boldsymbol{\theta}_j)\odot\mathbf{a}_{\mathrm{TE}}(\boldsymbol{\theta}_j)\right\|\le\gamma,\quad \bar{\boldsymbol{\theta}}_j\in\bar{\boldsymbol{\Omega}},\ j=1,\ldots,J \tag{4.17b}$$

$$\left|\mathbf{a}_{\mathrm{T}}^H\left(\boldsymbol{\vartheta}_0,f_d^0\right)\mathbf{C}\bar{\boldsymbol{\chi}}\left((\Delta\tau)_p,(\Delta f_d)_q\right)\mathbf{a}_{\mathrm{TE}}\left(\boldsymbol{\vartheta}_{\tilde{i}},(f_d)_q\right)\right|\le\delta \tag{4.17c}$$

$$(\Delta\tau)_p\in\mathfrak{D},\ p=1,\ldots,P$$

$$(\Delta f_d)_q\in\mathfrak{F},\ q=1,\ldots,Q$$

$$\boldsymbol{\vartheta}_{\tilde{i}}\in\widetilde{\boldsymbol{\Omega}},\ \tilde{i}=1,\ldots,\tilde{I}$$

$$\mathbf{a}_{\mathrm{T}}^H\left(\boldsymbol{\vartheta}_0,f_d^0\right)\mathbf{C}\mathbf{a}_{\mathrm{TE}}\left(\boldsymbol{\vartheta}_0,f_d^0\right)=K \tag{4.17d}$$

where $\boldsymbol{\vartheta}_0$ and $f_d^0$ are respectively the spatial angular vector and the Doppler frequency of the target, $\widetilde{\boldsymbol{\Omega}}$ combines the spatial region of interest where the AF sidelobes need to be suppressed using $\tilde{I}$ grids of spatial directions $\{\boldsymbol{\vartheta}_{\tilde{i}} \in \widetilde{\boldsymbol{\Omega}}, \tilde{i} = 1, \ldots, \tilde{I}\}$, $\{(\Delta\tau)_p \in \boldsymbol{\mathfrak{D}}, p = 1, \ldots, P\}$ and $\{(\Delta f_d)_q \in \boldsymbol{\mathfrak{F}}, q = 1, \ldots, Q\}$ are grids of delay and Doppler used to approximate the sectors-of-interest $\boldsymbol{\mathfrak{D}}$ and $\boldsymbol{\mathfrak{F}}$ by finite numbers of $P$ and $Q$ delay and Doppler bins, respectively, $(f_d)_q \triangleq (\Delta f_d)_q + f_d^0$, $\delta$ is the parameter of user choice that characterizes the sidelobe levels of the AF in the intersection of $\boldsymbol{\mathfrak{D}}$, $\boldsymbol{\mathfrak{F}}$, and $\widetilde{\boldsymbol{\Omega}}$, and $\odot$ denotes the element-wise product. It is worth noting that for a certain set of designed waveforms and a fixed group of parameters $((\Delta\tau)_p, (\Delta f_d)_q)$, $p \in \{1, \ldots, P\}$ and $q \in \{1, \ldots, Q\}$, the matrix $\bar{\boldsymbol{\chi}}((\Delta\tau)_p, (\Delta f_d)_q)$ in (4.17) can be easily known from (4.13). This motivates us to further explore the "clear region" bound of the TB-based MIMO radar AF which is studied in the next chapter.

# 5 "Clear region" analysis of the TB-based MIMO radar AF

The Siebert's self-transform property [20] expressed by the following equality

$$|\bar{\chi}(\sigma,\nu)|^2 = \iint_{-\infty}^{\infty} |\bar{\chi}(\tau, f_d)|^2 \exp\{-j2\pi\nu\tau + j2\pi f_d\sigma\}\mathrm{d}\tau\mathrm{d}f_d \tag{5.1}$$

holds for the Woodward's AF, and it is required that the transform (5.1) be non-negative when conducting the "clear region" analysis [19]. Here $\bar{\chi}(\sigma,\nu)$ is the new Woodward's AF generated from (4.12) by replacing the parameters $\tau$ and $f_d$ with $\sigma$ and $\nu$, respectively. In the context of the TB-based MIMO radar, let $f(\sigma,\nu)$ denote the self-transform of its AF $\chi(\boldsymbol{\Theta},\boldsymbol{\Theta'})$, i.e.,

$$f(\sigma,\nu) = \iint_{-\infty}^{\infty} \chi(\boldsymbol{\Theta},\boldsymbol{\Theta}')\exp\{-j2\pi\nu\Delta\tau + j2\pi\Delta f_d\sigma\}\mathrm{d}\Delta\tau\mathrm{d}\Delta f_d. \tag{5.2}$$

Normally, the TB-based MIMO radar AF (4.14) has negative terms in its expansion. Therefore, the transform (5.2) contains negative terms. Realizing this fact, it becomes clear that in general it is not guaranteed that $f(\sigma,\nu)$ is non-negative. However, it is needed in order to derive the "clear region" bound of the TB-based MIMO radar AF. Hence, to see how large the maximum achievable "clear region" of the TB-based MIMO radar AF is, we identify two limiting cases which both enable $f(\sigma,\nu)$ to be non-negative. In the first case, we only consider the squared AF terms in the expansion of (4.14). It is later shown that this case achieves the smallest "clear region" and has high relative sidelobe levels. Thus, it can be considered as the worst-case for the "clear region" bound of the TB-based MIMO radar AF defined in this thesis. In the second case, we assume that all the cross-AFs of the $K$ waveforms are zero, i.e., we can ignore the effects of the components in the AF expansion of (4.14) that are associated with the sidelobes resulting from different pairs of waveforms. This case represents the best situation for the "clear region" bound of the TB-based MIMO radar AF. However, it can never be achieved because in general more than one waveforms is transmitted in the TB-based MIMO radar system. The actual maximum achievable "clear region" bound of the TB-based MIMO radar AF is in between that of these two cases, and it depends on the level of the non-squared terms of the AF expansion which are windowed by the coherent processing gains and the equivalent transmit phase terms.

In the remaining part of this chapter, we analyze the worst- and best-case "clear

region". We first derive the bounds for these two cases, then we conduct the analysis based on these two bounds. The superscripts $(\cdot)^{\mathrm{I}}$ and $(\cdot)^{\mathrm{II}}$ are used for denoting the quantities with respect to the worst- and best-cases, respectively.

## 5.1 Worst-case bound

In the worst-case, in order to find the maximum achievable sidelobe-free area in Doppler-delay domain, we specify the following relaxed conditions on the auto- and cross-AFs

$$\begin{cases} \iint_A |[\bar{\boldsymbol{\chi}}]_{jj}(\tau, f_d)|^2 \mathrm{d}\tau \mathrm{d}f_d \simeq \iint\limits_{(0,0)} |[\bar{\boldsymbol{\chi}}]_{jj}(\tau, f_d)|^2 \mathrm{d}\tau \mathrm{d}f_d \triangleq V_j \\ \iint_A |[\bar{\boldsymbol{\chi}}]_{jk, j\neq k}(\tau, f_d)|^2 \mathrm{d}\tau \mathrm{d}f_d \simeq 0 \end{cases} \tag{5.3}$$

where $A$ denotes the convex and centrosymmetric region of integration in the Doppler-delay plane. Here, we define the volume of the TB-based MIMO radar AF over the integral region $A$ as

$$V_{\mathrm{TB}}(A) \triangleq \iint_A \chi(\boldsymbol{\Theta}, \boldsymbol{\Theta}') \mathrm{d}\Delta\tau \mathrm{d}\Delta f_d. \tag{5.4}$$

In the following derivation, we assume that all the $K$ waveforms are sharing the same bandwidth and time duration, meaning that the integration of the auto-AF for each waveform over region $A$ has a fixed volume $V_0$, i.e., $V_j = V_0$, $\forall j \in \{1, \ldots, K\}$. By substituting (4.14) into (5.4), the volume of the TB-based MIMO radar AF for the worst-case scenario can be expressed as

$$\begin{aligned} V_{\mathrm{TB}}^{\mathrm{I}}(A) &\simeq \frac{E}{K} \left| \mathbf{a}_{\mathrm{R}}^H(\boldsymbol{\Theta}) \mathbf{a}_{\mathrm{R}}(\boldsymbol{\Theta}') \right|^2 \iint_A \left( \sum_{k=1}^{K} |\Upsilon_k|^2 \right) |[\bar{\boldsymbol{\chi}}]_{kk}(\Delta\tau, \Delta f_d)|^2 \mathrm{d}\Delta\tau \mathrm{d}\Delta f_d \\ &= \frac{E}{K} \left| \mathbf{a}_{\mathrm{R}}^H(\boldsymbol{\Theta}) \mathbf{a}_{\mathrm{R}}(\boldsymbol{\Theta}') \right|^2 \left( \sum_{k=1}^{K} |\Upsilon_k|^2 \right) V_0 \qquad (5.5) \\ &\triangleq V_K \qquad (5.6) \end{aligned}$$

where $\Upsilon_k \triangleq \mathbf{a}_{\mathrm{T}}^H(\boldsymbol{\Theta}) \mathbf{c}_k$, $k \in \{1, \ldots, K\}$ is the $k$th coherent processing gain that has been defined before.

Employing the Siebert's self-transform property (5.1) and Parseval's theorem, under the condition that $\psi(\tau, f_d)$ is any quadratically integrable function whose

Fourier transform is

$$\Psi(\tau, f_d) = \iint_{-\infty}^{\infty} \psi(\sigma, \nu) \exp\{-j2\pi\nu\tau + j2\pi f_d \sigma\} \mathrm{d}\sigma \mathrm{d}\nu \tag{5.34}$$

the following transform

$$\begin{aligned}
&\iint_A \chi(\boldsymbol{\Theta}, \boldsymbol{\Theta}') \phi(\Delta\tau, \Delta f_d) \mathrm{d}\Delta\tau \mathrm{d}\Delta f_d \\
&= \frac{E}{K} \iint_{A'} \left| \mathbf{a}_{\mathrm{R}}^H(\boldsymbol{\Theta}) \mathbf{a}_{\mathrm{R}}(\boldsymbol{\Theta}') \right|^2 \sum_{k=1}^{K} \sum_{j=1}^{K} |\Upsilon_k \mathbf{a}_{\mathrm{TE}}(j)|^2 \\
&\qquad \times [\bar{\boldsymbol{\chi}}]_{kk}^*(\Delta\tau, \Delta f_d) [\bar{\boldsymbol{\chi}}]_{jj}(\Delta\tau, \Delta f_d) \Psi(\Delta\tau, \Delta f_d) d\Delta\tau d\Delta f_d \\
&\triangleq V_{\mathrm{TB}}^{\mathrm{I}'}(A')
\end{aligned} \tag{5.35}$$

holds.

Under the assumption that $A$ is convex, symmetric around the origin, and furthermore contains a delta function at the origin, it can be shown using the approach in [19] that the following inequality

$$\begin{aligned}
V_{\mathrm{TB}}^{\mathrm{I}}(A) &> \frac{1}{4} C(A) \lim_{A' \to 0} V_{\mathrm{TB}}^{\mathrm{I}'}(A') \\
&= \frac{1}{4} C(A) \frac{N^2 \left( \sum_{k=1}^{K} \sum_{j=1}^{K} |\Upsilon_k \mathbf{a}_{\mathrm{TE}}(j)|^2 \right)}{|\mathbf{a}_{\mathrm{R}}^H(\boldsymbol{\Theta}) \mathbf{a}_{\mathrm{R}}(\boldsymbol{\Theta}')|^2 \left( \sum_{k=1}^{K} |\Upsilon_k|^2 \right)} V_K \\
&= \frac{1}{4} C(A) \frac{N^2 K}{|\mathbf{a}_{\mathrm{R}}^H(\boldsymbol{\Theta}) \mathbf{a}_{\mathrm{R}}(\boldsymbol{\Theta}')|^2} V_K
\end{aligned} \tag{5.36}$$

holds, where $C(A)$ denotes the area of $A$, and $V_K$ is defined in (5.5).

Based on (5.36) and considering the "$\eta$-clear" area that is convex and symmetric around the origin with $\chi(\boldsymbol{\Theta}, \boldsymbol{\Theta}') \leq \eta$, we obtain that the following inequality for the worst-case "clear region" of the TB-based MIMO radar AF

$$C_{\mathrm{TB}}^{\mathrm{I}}(A) \leq \frac{4V_K}{\frac{N^2 K}{\left| \mathbf{a}_{\mathrm{R}}^H(\boldsymbol{\Theta}) \mathbf{a}_{\mathrm{R}}(\boldsymbol{\Theta}') \right|^2} V_K - 4\eta} \tag{5.37}$$

which holds if and only if

$$\eta < \frac{N^2 K V_K}{4 |\mathbf{a}_{\mathrm{R}}^H(\boldsymbol{\Theta}) \mathbf{a}_{\mathrm{R}}(\boldsymbol{\Theta}')|^2}. \tag{5.38}$$

## 5.2 Best-case bound

In the best-case, based on the same assumptions for the transmitted waveforms as made in the worst-case, and using also (4.14), (5.4) can be expressed as

$$V_{\mathrm{TB}}^{\mathrm{II}}(A) = V_{\mathrm{TB}}^{\mathrm{I}}(A) \simeq V_K. \tag{5.39}$$

Similarly, the following transform

$$\begin{aligned}
&\iint_A \chi(\boldsymbol{\Theta}, \boldsymbol{\Theta}')\psi(\Delta\tau, \Delta f_d)\mathrm{d}\Delta\tau\mathrm{d}\Delta f_d \\
&= \frac{E}{K}\iint_{A'} \left|\mathbf{a}_{\mathrm{R}}^H(\boldsymbol{\Theta})\mathbf{a}_{\mathrm{R}}(\boldsymbol{\Theta}')\right|^2 \sum_{k=1}^{K}|\Upsilon_k|^2|[\bar{\boldsymbol{\chi}}]_{kk}(\Delta\tau, \Delta f_d)|^2\Psi(\Delta\tau, \Delta f_d)\mathrm{d}\Delta\tau\mathrm{d}\Delta f_d \\
&\triangleq V_{\mathrm{TB}}^{\mathrm{II}'}(A')
\end{aligned} \tag{5.40}$$

holds. Under the same condition as applied in the worst-case, it can be shown that the following inequality

$$\begin{aligned}
V_{\mathrm{TB}}^{\mathrm{II}}(A) &> \frac{1}{4}C(A)\lim_{A'\to 0} V_{\mathrm{TB}}^{\mathrm{II}'}(A') \\
&= \frac{1}{4}C(A)\frac{N^2\left(\sum_{k=1}^{K}|\Upsilon_k|^2\right)}{\left|\mathbf{a}_{\mathrm{R}}^H(\boldsymbol{\Theta})\mathbf{a}_{\mathrm{R}}(\boldsymbol{\Theta}')\right|^2\left(\sum_{k=1}^{K}|\Upsilon_k|^2\right)}V_K \\
&= \frac{1}{4}C(A)\frac{N^2}{\left|\mathbf{a}_{\mathrm{R}}^H(\boldsymbol{\Theta})\mathbf{a}_{\mathrm{R}}(\boldsymbol{\Theta}')\right|^2}V_K
\end{aligned} \tag{5.41}$$

holds.

Based on (5.41) and considering the "$\eta$-clear" area that is convex and symmetric around the origin for $\chi(\boldsymbol{\Theta}, \boldsymbol{\Theta}') \leq \eta$, we obtain the following inequality for the best-case "clear region" of the TB-based MIMO radar AF

$$C_{\mathrm{TB}}^{\mathrm{II}}(A) \leq \frac{4V_K}{\frac{N^2}{\left|\mathbf{a}_{\mathrm{R}}^H(\boldsymbol{\Theta})\mathbf{a}_{\mathrm{R}}(\boldsymbol{\Theta}')\right|^2}V_K - 4\eta} \tag{5.42}$$

which holds if and only if

$$\eta < \frac{N^2V_K}{4\left|\mathbf{a}_{\mathrm{R}}^H(\boldsymbol{\Theta})\mathbf{a}_{\mathrm{R}}(\boldsymbol{\Theta}')\right|^2}. \tag{5.43}$$

## 5.3 Discussion

The worst- and best-case "clear region" bounds in (5.37) and (5.42) which correspond to the two identified limiting cases indicate that they depend on the array configuration, and the quantity $N^2/|\mathbf{a}_R^H(\boldsymbol{\Theta})\mathbf{a}_R(\boldsymbol{\Theta}')|^2$ makes these two bounds variable. The smaller the quantity is, the larger the maximum possible "clear region" bound can be obtained. The largest bound is achieved when this quantity is decreased to 1 as long as the $\eta$-level condition is guaranteed.

The "clear region" bound for the worst-case indicates that the worst achievable "clear region" of the TB-based MIMO radar AF is independent of the coherent gains, however, it depends on the number of transmitted waveforms $K$ under the condition that the emitted waveforms share the same characteristic parameters and have the same properties. In this sense, it is similar to the case of the traditional MIMO radar AF with $K$ mutually orthogonal waveforms that has been given in [23]. However, the worst-case bound derived here clarifies that the worst-case "clear region" of the TB-based MIMO radar AF is inversely proportional to the number of orthogonal waveforms $K$ (or the number of beams), but not the number of transmit antenna elements $M$. Contrarily, the best-case "clear region" bound indicates that the ideal "clear region" for the TB-based MIMO radar AF is independent of the waveform number $K$, and it is equivalent to the case of the PA radar AF with a single waveform that has been shown in [19].

It is worth noting from analyzing (5.5) that $V_K$ defined in (5.6) is partially determined by the sum of squared magnitudes of the coherent processing gains $\Upsilon_k$, $k = 1, \ldots, K$, which means that it is subjected to the TB matrix $\mathbf{C}$ employed by the TB-based MIMO radar system. This quantity, together with the one resulted from the receive array geometry, determines how small the $\eta$-level can be for the TB-based MIMO radar AF. The PA radar and the traditional MIMO radar have their own fixed forms of the TB matrices. Therefore, their AFs achieve fixed values of volume $V_K$ under the conditions (5.3). Different from the former two, the TB-based MIMO radar uses its own TB matrix $\mathbf{C}$, which makes its maximum "clear region" varying in the range bounded by the worst- and best-case bounds. This leads to significant differences between the results achieved for the traditional MIMO radar AF in [23] and that achieved for the TB-based MIMO radar AF.

The actual maximum achievable "clear region" of the TB-based MIMO radar AF is bounded on both sides by the two identified limiting cases. The worst-case bound becomes larger as $K$ decreases. Consequently, there exists a tradeoff between the

maximum achievable "clear region" and the waveform diversity for the TB-based MIMO radar AF. Once the desired radar system and target parameters are selected, the TB-based MIMO radar AF can be evaluated directly using its definition (4.6) or simplification (4.14). This facilitates the radar designer to find the best tradeoff. The worst- and best-case bounds derived in (5.37) and (5.42) also implicate that the traditional MIMO radar AF achieves the worst maximum achievable "clear region", and it is approximately $1/M$ that of the PA radar, which agrees with the result of [23]. It is clear that the maximum achievable "clear region" of the TB-based MIMO radar AF is in between that of the PA and traditional MIMO radar cases.

There exist waveform design methods based on minimizing or explicitly constraining the sidelobe levels of the transmitted waveforms [22, 40, 45]. Hence, large "clear region" under the "$\eta$-clear" condition can be achieved. To further obtain a larger "clear region" for the TB-based MIMO radar AF, one can resort to the range-Doppler sidelobes mitigation techniques. For example, receiver instrumental variable filter [45, 107, 108] can be employed at the receiving end to suppress the sidelobes. However, the attainable "clear region" depends on the exact sidelobe mitigation level.

# 6 Simulation results and analyses

In this chapter, we provide numerical examples in order to demonstrate the AFs for different radar configurations using the generalized TB-based MIMO radar AF definition given in this thesis. Meanwhile, we also present the comparison between the two AF metrics defined in this thesis and [23].

Throughout the simulations, we assume that uniform linear arrays of $M = 8$ omni-directional transmit antenna elements and $N = 8$ omni-directional receive elements spaced half a wavelength apart from each other are used. Both the transmit and receive arrays are located on the $x$-axis with their centers being located at the origin. The total transmit energy $E$ is fixed to be equal to the number of the transmit antenna elements $M$. Two types of waveforms are employed for each simulation example. One is in the form of polyphase-coded sequence [109], and the other is in the form of Gaussian sequence. Each waveform has the same wavelength that equals 256. We employ a single pulse for all the waveforms, and the pulse width $T$ is selected to be 10 ms. The time-bandwidth product $BT$ is set to be equal to 128, and the sampling rate $f_s$ is selected to be two times of the bandwidth, i.e., $f_s = 2B$. For the simulation results, we show the 2D (side view) results with polyphase-coded waveforms in the first sub figure and three-dimensional (3D) (full view) result with Gaussian waveforms in the second sub figure of each example. We fix both target parameters $\mathbf{\Theta}$ (with zero Doppler) and $\mathbf{\Theta}'$ in the $x$-$y$ plane, and the latter is varying. In the first four examples, both parameters are set to share the same spatial angle $\theta = 0°$. While in the last two examples, both parameters are set to share the same delay $\tau = 0$, but $\mathbf{\Theta}'$ is allowed to have different spatial angles. The maximum magnitudes of all the simulated AFs are normalized to 1, thus, the mainlobes of all the simulated AFs are 0 dB. We use the CVX MATLAB toolbox [110] to solve the convex optimization design problems in the last three examples.

## 6.1 Example 1: The difference between the TB-based MIMO radar AF and the square-summation-form AF metrics

In the first example, we show the AF difference between the normalized TB-based MIMO radar AF metric defined in this thesis and the AF metric defined in [23] (see Figure 6.1). The traditional MIMO radar configuration emitting 8 single-pulse polyphase-coded or Gaussian waveforms is employed. It can be seen from both sub figures that the differences are almost always positive, meaning that the relative

sidelobe levels of the AF in [23] are almost always higher than that obtained using the AF expression defined in this thesis. The largest difference of the relative sidelobe level for the two AF metrics reaches 4% of the normalized AF metric peak. It can be seen from Figure 6.1(a). that the major differences are present in the area around the AF mainlobe from the view of delay domain, and they appear in the whole area from the view of Doppler domain. This example verifies that the traditional MIMO radar AF metric defined in [23] leads to higher relative sidelobe levels, and it can serve as the worst-case for the TB-based MIMO radar AF.

## 6.2 Example 2: The difference between the TB-based and traditional MIMO radar AFs using the generalized AF definition

In the second example, we show the AF difference between the normalized TB-based MIMO radar AF and the traditional MIMO radar AF using the AF metric defined in this thesis (see Figure 6.2). For the TB-based MIMO radar AF, we employ the first 4 waveforms of each type. The corresponding TB matrix $\mathbf{C}$ is designed to satisfy the condition that the coherent gains are of the same magnitude, but have different phases, i.e., the RIP at the receive array is satisfied [14]. For the traditional MIMO radar AF, all 8 waveforms of both types are used. The corresponding TB matrix $\mathbf{C}$ is selected as an identity matrix. It can be seen from both sub figures that the difference levels almost always lie far within $\pm 1\%$ of the normalized AF peak, especially from the view of delay domain, meaning that the TB-based MIMO radar AF can achieve the same or lower levels of relative sidelobes compared to that for the traditional MIMO radar configuration. It can be seen that these differences are smaller than the difference shown in Figure 6.1. In the following examples, it can be seen that the different levels ($\pm 1\%$ versus 4%) result in big differences of relative sidelobe levels (up to 30 dB for the biggest one).

## 6.3 Example 3: The square-summation-form traditional MIMO radar AF

In the third example, we show the square-summation-form traditional MIMO radar AF metric defined in [23] using the aforementioned two types of 8 waveforms (see Figure 6.3). It can be seen from both the 2D and 3D results that the relative sidelobe levels of the AF using this definition are very high, ranging from about $-40$ dB to

$-10$ dB, and they concentrate to the range from about $-20$ dB to $-10$ dB which is identified in both sub figures by the dark red area. From the view of delay domain, it can be seen that all the AF sidelobes in the range of delays from $-6$ ms to 6 ms are above $-20$ dB, and the highest level of sidelobes around the AF mainlobe reaches approximately $-13$ dB. While from the view of Doppler domain, it can be seen that most of the AF sidelobes concentrate on the range from about $-23$ dB to $-14$ dB, and they appear in the whole area because the waveforms are designed without considering Doppler tolerance. The worst sidelobe level from this view reaches approximately $-10$ dB. To maintain good Doppler tolerance, we can also enforce spectral constraints [106] besides ensuring good waveform correlation (i.e., zero-Doppler cut of AF) property when designing the waveforms. However, this is beyond the scope of our paper. We aim at showing how the simulated AFs with different definitions behave. Hence, together with the result in Figure 6.1, this example implicates that the square-summation-form AF metric obtains worse "clear region" than that of the AF defined in this thesis for a given allowable sidelobe level limit $\eta$. In other words, the sidelobe level limit for the AF in [23] can only be set to a relatively high value as compared to that for the defined TB-based MIMO radar AF metric in this thesis.

## 6.4 Example 4: The TB-based MIMO radar AF with the first TB design

In the fourth example, we show the TB-based MIMO radar AF (see Figure 6.4). The first 4 waveforms of each type are selected in this simulation, therefore, the TB matrix $\mathbf{C}$ is of size $8 \times 4$. We use the convex optimization strategy (3.18) to design the TB matrix $\mathbf{C}$. The target velocity is not needed when carrying out the optimization process, thus we employ the spatial angle $\theta$ to replace the parameter $\boldsymbol{\Theta}$ in all the steering vectors. The transmit energy is focused within the spatial sector $\boldsymbol{\Omega} = [-15^\circ, 15^\circ]$ via 4 transmit beams, the RIP is guaranteed by selecting the presumed vector as $\mathbf{d}(\theta) = [\exp\{\mu_1(\theta)\}, \ldots, \exp\{\mu_4(\theta)\}]^T$ where $\mu_k(\theta)$, $k \in \{1, \ldots, 4\}$ is the $k$th linear function of the spatial angle $\theta$, and the parameter that controls the level of radiated power outside $\boldsymbol{\Omega}$ is selected as $\gamma = 0.38$. It can be seen from both sub figures that the relative sidelobes of the TB-based MIMO radar AF are dispersive. From the view of delay domain, it can be seen that the major sidelobes around the AF mainlobe concentrate on the level of $-20$ dB. While from the view of Doppler domain, it can be seen that the average level of

major sidelobes is about $-20$ dB. The worst sidelobe level from this view is about $-12$ dB, which is because the convex optimization design (3.18) does not consider the factor of Doppler processing. It can also be seen from both views that the lowest sidelobe level which is below $-70$ dB is much smaller compared to that in the last example.

## 6.5 Example 5: The TB-based MIMO radar AF with the second TB design

In the fifth example, we show the TB-based MIMO radar AF versus Doppler and spatial angles (see Figure 6.5). The convex optimization strategy (3.18) is still used to design the TB matrix $\mathbf{C}$. All other simulation parameters are the same as that used in the last example except the parameter $\gamma$ is selected as 0.2. To better display the result, we remove all the sidelobes that are below $-90$ dB. It can be seen from the 3D sub figure that the TB-based MIMO radar AF has lower sidelobe levels versus angles than that versus Doppler. From the view of angle, the AF indeed shows the beampattern of the TB-based MIMO radar system, and the highest relative sidelobe level in this view is about $-20$ dB. From the view of Doppler, the worst relative sidelobe level is approximately 2 dB better than that in the last example, i.e., it decrease to about $-14$ dB. However, it is still high due to the reason that the design of the TB matrix does not consider the factor of Doppler processing.

## 6.6 Example 6: The TB-based MIMO radar AF with the third TB design

In the last example, we show the TB-based MIMO radar AF versus Doppler and spatial angles using the proposed TB strategy (4.17) (see Figure 6.6). We aim at suppressing the relative AF sidelobe levels in the ranges $[-0.2\,\text{kHz}, -0.1\,\text{kHz}] \cup [0.1\,\text{kHz}, 0.2\,\text{kHz}]$ at the spatial direction of $\theta = 0^\circ$. The parameters $\gamma$ and $\delta$ are respectively selected as $\gamma = 0.1$ and $\delta = 0.32$, $\boldsymbol{\vartheta} = \mathbf{0}^\circ$, and $f_d^0 = 0\,\text{kHz}$. All other simulation parameters are the same as that used in the fourth example. To better display the result, we also remove the sidelobes that are below $-90$ dB. It can be seen from the 2D sub figure that the worst sidelobe level in the desired Doppler ranges is well suppressed to below $-17$ dB, and the worst sidelobe level in the whole Doppler domain which is far away from the AF mainlobe is about $-15$ dB. Because there is no constraint on the sidelobe levels versus other angles except $\theta = 0^\circ$ in (4.17), the

worst sidelobe level in the whole spatial domain increases to about $-15$ dB. The 3D results with Gaussian waveforms, indeed, show much lower Doppler sidelobe levels in the desired ranges. This example verifies the tradeoffs in the TB-based MIMO radar [33]. If more degrees of freedom are available in the TB-based MIMO radar, for example, more antennas are employed, then more flexible relative sidelobe levels can be achieved.

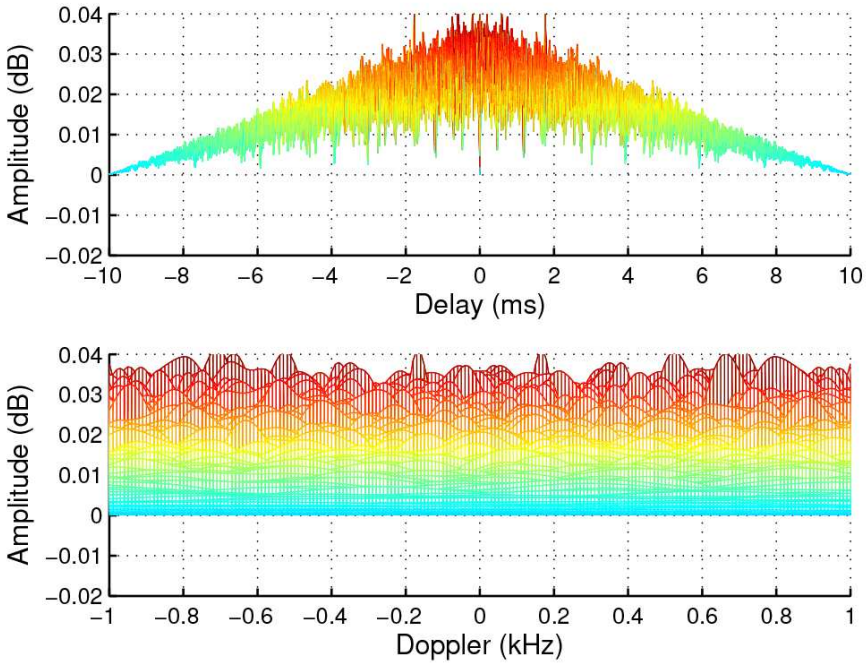


(a)

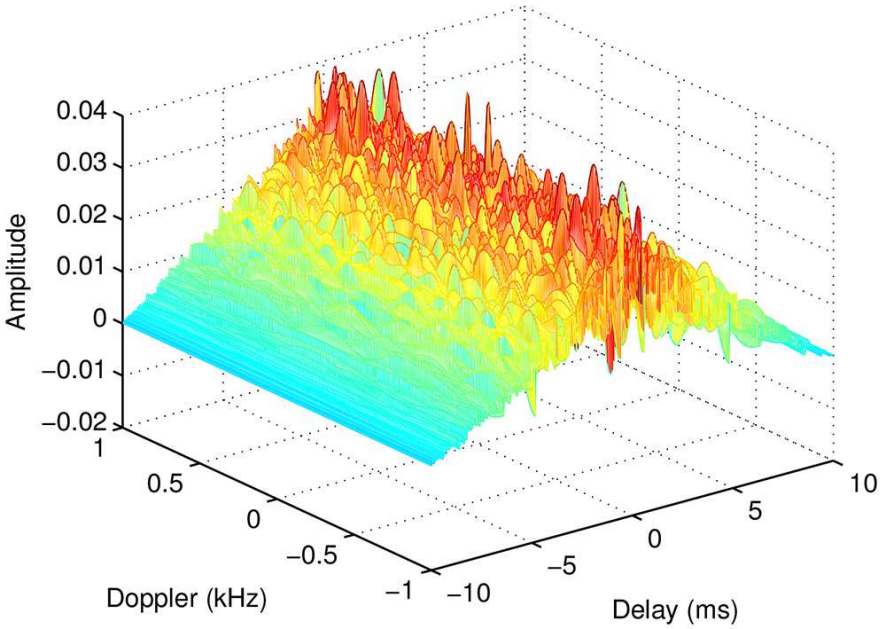


(b)

Figure 6.1: The difference between the defined TB-based MIMO radar AF metric in this thesis and the square-summation-form AF metric defined in [23]. Here $M = 8$, $N = 8$, $K = 8$, and $E = M$. 8 single-pulse waveforms for the traditional MIMO radar case are used: $T = 10$ ms, $BT = 128$, and $f_s = 2B$. $\mathbf{C}$ is given as the identity matrix $\mathbf{I}_M$. (a) Polyphase-coded waveforms (b) Gaussian waveforms. Positive difference means that the AF defined in [23] has higher relative sidelobe levels.

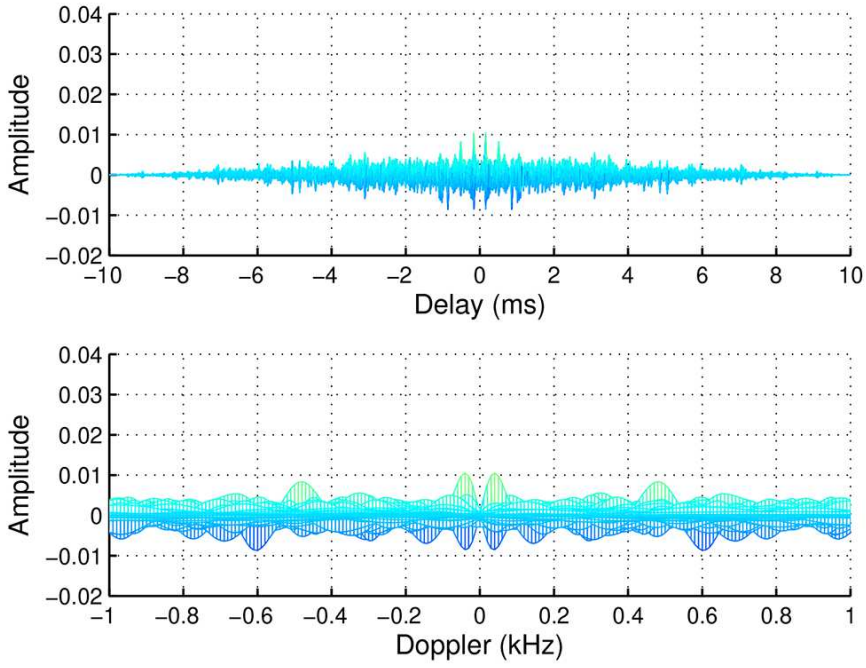


(a)

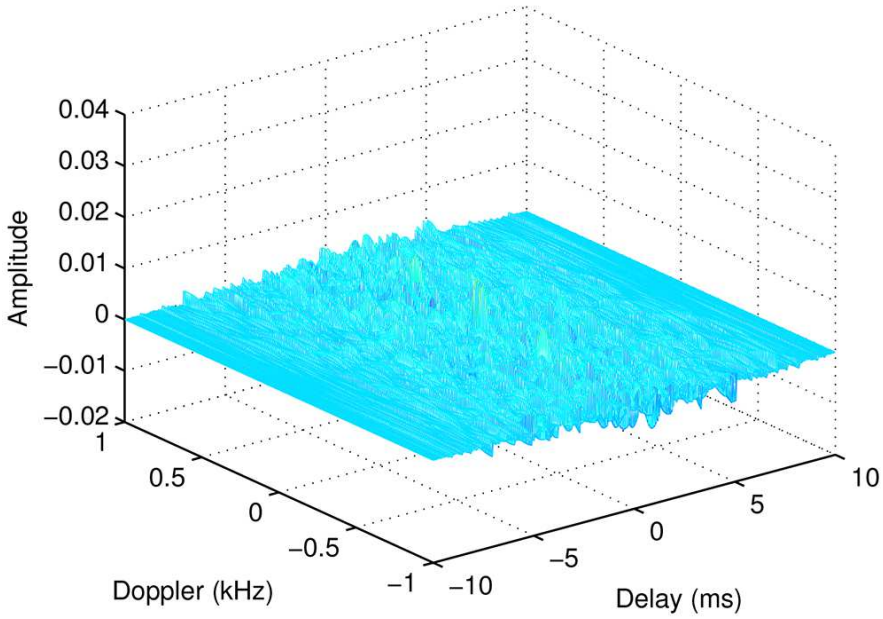


(b)

Figure 6.2: The difference between the TB-based and traditional MIMO radar AFs using the generalized AF definition in this thesis. Here $M = 8$, $N = 8$, and $E = M$. The first 4 single-pulse waveforms are used: $T = 10$ ms, $BT = 128$, $f_s = 2B$. $\mathbf{C}$ is designed to guarantee the rotational invariance property. The traditional MIMO radar AF uses the total 8 waveforms and employs $\mathbf{C}$ as an identity matrix. (a) Polyphase-coded waveforms (b) Gaussian waveforms.

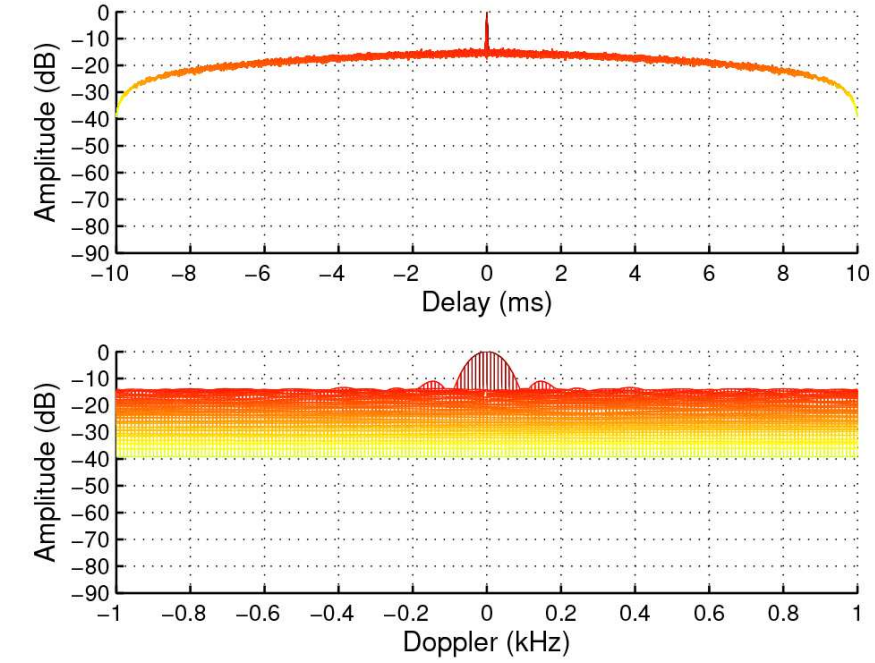


(a)

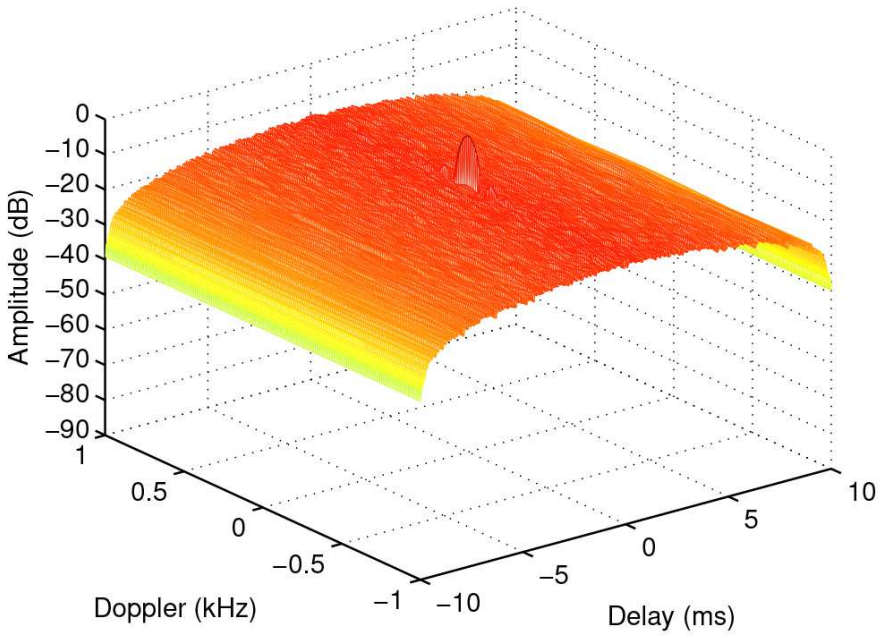


(b)

Figure 6.3: The square-summation-form traditional MIMO radar AF defined in [23]. Here $M = 8$, $N = 8$, and $E = M$. The total eight single-pulse waveforms are used: $T = 10$ ms, $BT = 128$, and $f_s = 2B$. (a) Polyphase-coded waveform (b) Gaussian waveform. High relative sidelobe levels are achieved in Doppler-delay domain using this AF.

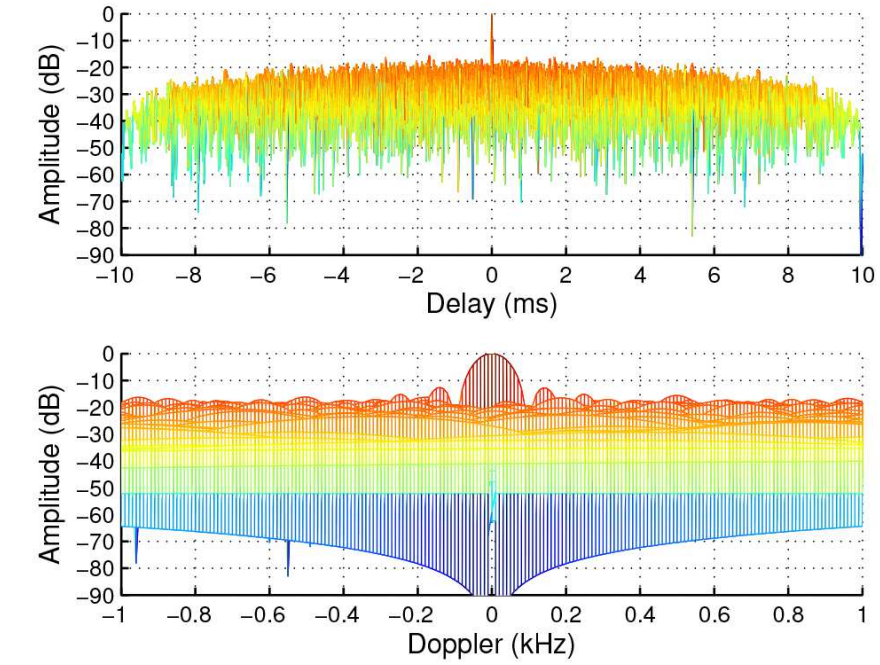


(a)

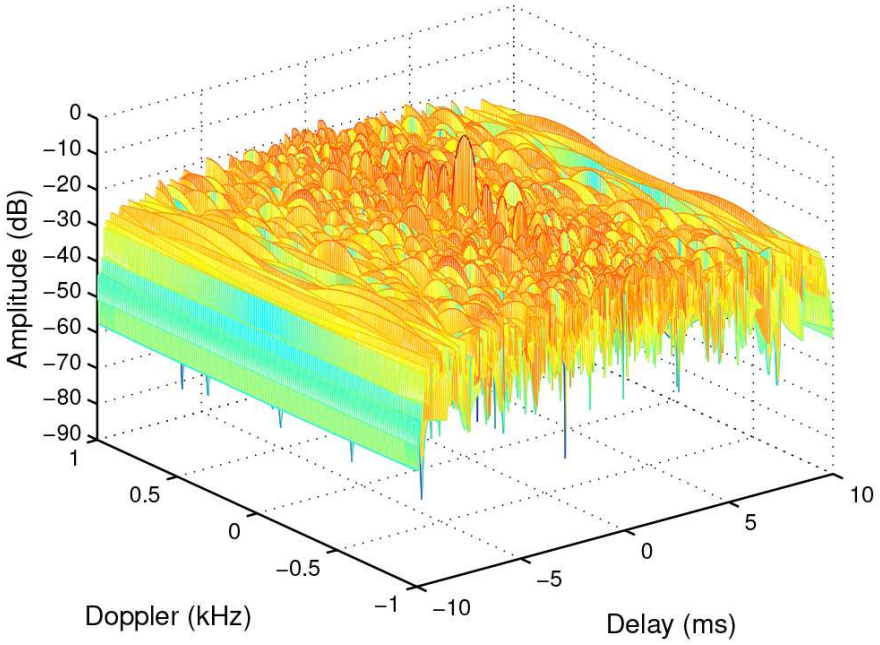


(b)

Figure 6.4: The TB-based MIMO radar AF with the first TB design. Here $M = 8$, $N = 8$, $K = 8$, and $E = M$. The first four single-pulse waveforms are used: $T = 10$ ms, $BT = 128$, and $f_s = 2B$. $\mathbf{C}$ is designed using the convex optimization method (3.18). (a) Polyphase-coded waveforms (b) Gaussian waveforms. Low relative sidelobe levels are achieved in Doppler-delay domain using this AF.

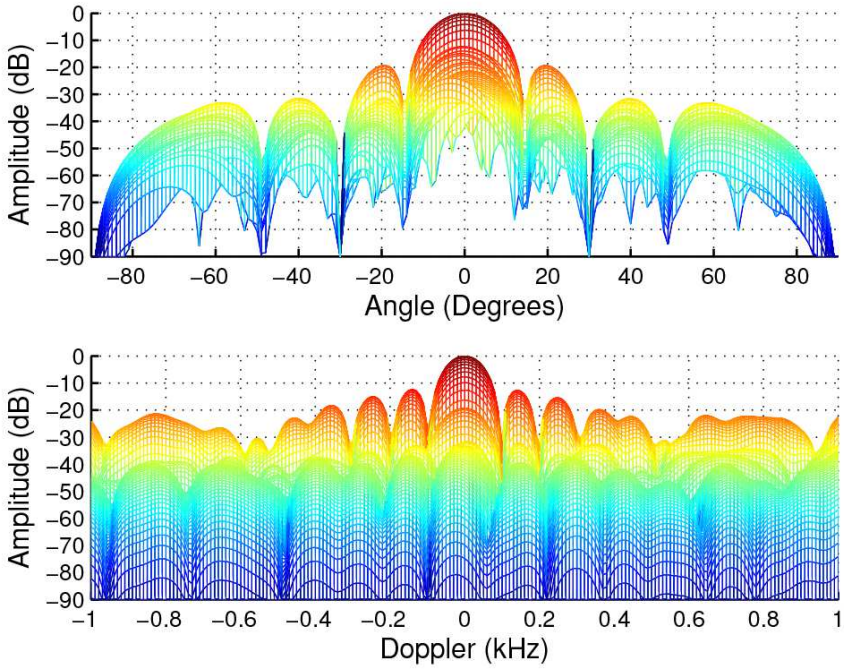


(a)

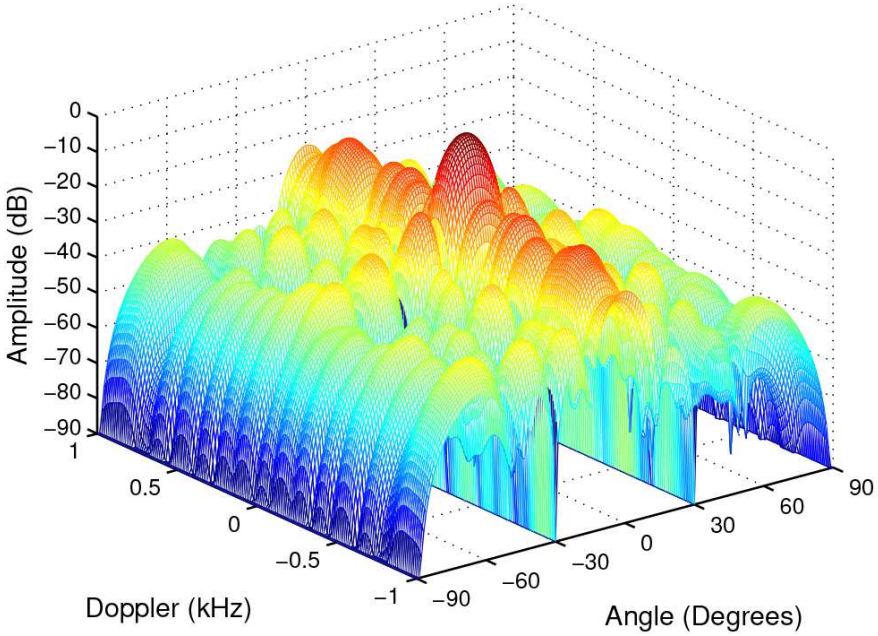


(b)

Figure 6.5: The TB-based MIMO radar AF with the second TB design. Here $M = 8$, $N = 8$, $K = 4$, and $E = M$. The first four single-pulse waveforms are used: $T = 10$ ms, $BT = 128$, and $f_s = 2B$. $\mathbf{C}$ is designed using the convex optimization method (3.18). (a) Polyphase-coded waveforms (b) Gaussian waveforms. Low level relative sidelobe levels of AF are achieved.

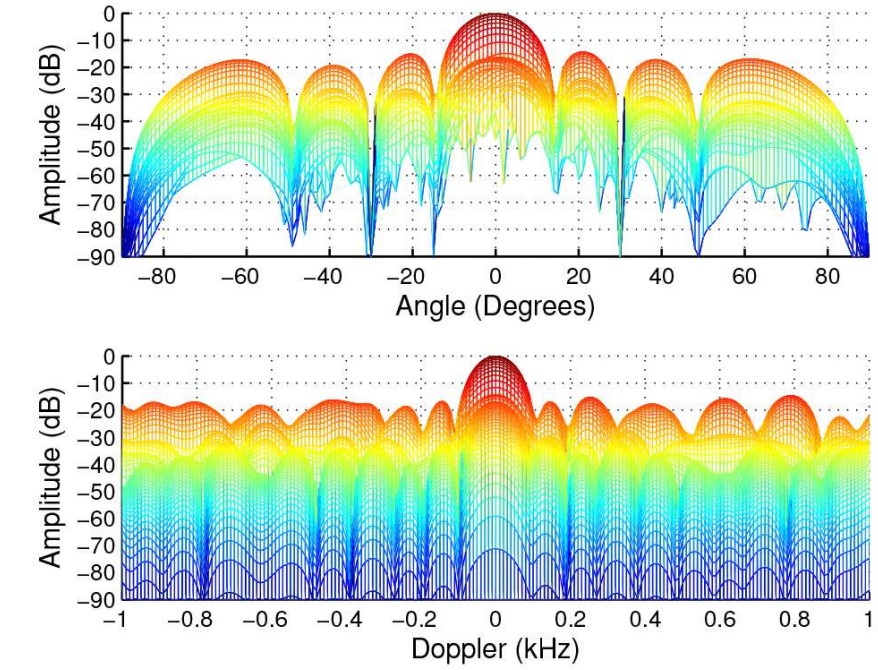


(a)

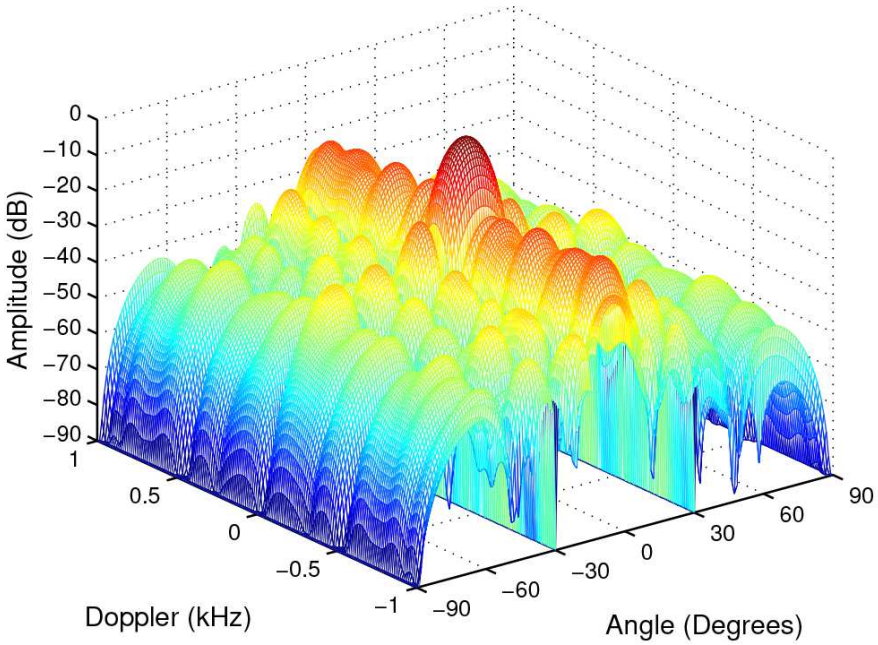


(b)

Figure 6.6: The TB-based MIMO radar AF with the third TB design. Here $M = 8$, $N = 8$, $K = 4$, and $E = M$. The first four single-pulse waveforms are used: $T = 10$ ms, $BT = 128$, and $f_s = 2B$. $\mathbf{C}$ is designed using the convex optimization method (4.17). (a) Polyphase-coded waveforms (b) Gaussian waveforms. Relative sidelobe levels of AF in Doppler domain are further suppressed.

# 7 Summary

In this thesis, we have derived the AF for the recently proposed TB-based MIMO radar which allows for obtaining waveform diversity and coherent processing gains over a pre-defined angular sector simultaneously. Our definition is very general and contains the AFs for the PA, traditional MIMO, and TB-based MIMO radars as important special cases under the standard assumption of far-field targets narrowband waveforms. Relationships among the TB-based MIMO radar AF defined in this thesis and the previous AF works including the Woodward's AF, the AF defined for the traditional colocated MIMO radar, and the PA radar AF, have been established, respectively. We have compared our newly defined TB-based MIMO radar AF with the existing traditional MIMO radar AFs, and have proposed a new TB design in order to give better relative AF sidelobe levels. Two limiting cases are identified to bound the "clear region" of the TB-based MIMO radar AF, and corresponding bounds for these two cases have been derived, respectively. We have shown that the "clear region" for the worst bounding case is inversely proportional to the number of transmitted waveforms $K$, while the one for the best bounding case is independent of $K$. The "clear region" of the TB-based MIMO radar AF, which depends on the array configuration, is in between that of the worst- and best-cases. We have shown in the simulation results that the square-summation-form AF leads to higher relative AF sidelobe levels than that of the TB-based MIMO radar AF. Moreover, using the proposed convex optimization TB design, the levels can be further reduced.

# References

[1] J. Li and P. Stoica, *MIMO Radar Signal Processing.* New York: Wiley, 2009.

[2] A. M. Haimovich, R. S. Blum, and L. J. Cimini, "MIMO radar with widely separated antennas," *IEEE Signal Processing Magazine*, vol. 24, no. 1, pp. 116–129, January 2008.

[3] J. Li and P. Stoica, "MIMO radar with colocated antennas," *IEEE Signal Processing Magazine*, vol. 24, no. 5, pp. 106–114, September 2007.

[4] E. Fishler, A. Haimovich, R. S. Blum, L. Cimini, D. Chizhik, and R. Valenzuela, "Spatial diversity in radars—Models and detection performance," *IEEE Transactions on Signal Processing*, vol. 54, no. 3, pp. 823–838, March 2006.

[5] E. Fishler, A. Haimovich, R. S. Blum, D. Chizhik, L. Cimini, and R. Valenzuela, "MIMO radar: An idea whose time has come," in *Proc. IEEE Radar Conference*, Honolulu, HI, April 2004, pp. 71–78.

[6] I. Bekkerman and J. Tabrikian, "Target detection and localization using MIMO radar and sonars," *IEEE Transactions on Signal Processing*, vol. 54, no. 10, pp. 3873–3883, October 2006.

[7] D. R. Fuhrmann, J. P. Browning, and M. Rangaswamy, "Signaling strategies for the hybrid MIMO phased-array radar," *IEEE Journal of Selected Topics in Signal Processing*, vol. 4, no. 1, pp. 66–78, September 2010.

[8] A. Hassanien and S. A. Vorobyov, "Transmit energy focusing for DOA estimation in MIMO radar with colocated antennas," *IEEE Transactions on Signal Processing*, vol. 59, no. 6, pp. 2669–2682, June 2011.

[9] D. R. Fuhrmann and G. S. Antonio, "Transmit bemforming for MIMO radar systems using signal cross-correlation," *IEEE Transactions on Aerospace and Electronic Systems*, vol. 44, no. 1, pp. 171–186, January 2008.

[10] P. Stoica, J. Li, and Y. Xie, "On probing signal design for MIMO radar," *IEEE Transactions on Signal Processing*, vol. 55, no. 8, pp. 4151–4161, August 2007.

[11] A. Hassanien and S. A. Vorobyov, "Phased-MIMO radar: A tradeoff between phased-array and MIMO radars," *IEEE Transactions on Signal Processing*, vol. 58, no. 6, pp. 3137–3151, June 2010.

[12] A. Khabbazibasmenj, A. Hassanien, S. A. Vorobyov, and M. W. Morency, "Efficient transmit beamspace design for search-free based DOA estimation in MIMO radar," *IEEE Transactions on Signal Processing*, vol. 62, no. 6, pp. 1490–1500, March 2014.

[13] A. Khabbazibasmenj, S. A. Vorobyov, A. Hassanien, and M. W. Morency, "Transmit beamspace design for direction finding in colocated MIMO radar with arbitrary receive array and even number of waveforms," in *Proc. Asilomar Conference on Signals, Systems, and Computers*, Pacific Grove, CA, November 2012, pp. 1307–1311.

[14] A. Khabbazibasmenj, S. A. Vorobyov, and A. Hassanien, "Transmit beamspace design for direction finding in colocated MIMO radar with arbitrary receive array," in *Proc. IEEE International Conference on Acoustics, Speech, and Signal Processing (ICASSP)*, Prague, Czech Republic, May 2011, pp. 2784–2787.

[15] T. Aittomaki and V. Koivunen, "Low-complexity method for transmit beamforming in MIMO radars," in *Proc. IEEE International Conference on Acoustics, Speech, and Signal Processing (ICASSP)*, vol. II, Honolulu, HI, April 2007, pp. 305–308.

[16] T. Aittomaki and V. Koivunen, "Signal covariance matrix optimization for transmit beamforming in MIMO radars," in *Proc. Asilomar Conference on Signals, Systems, and Computers*, Pacific Grove, CA, November 2007, pp. 182–186.

[17] R. O. Schmidt, "Multiple emitter location and signal parameter estimation," *IEEE Transactions on Antennas and Propagation*, vol. 34, no. 3, pp. 276–280, March 1986.

[18] R. Roy and T. Kailath, "ESPRIT—Estimation of signal parameters via rotational invariance techniques," *IEEE Transactions on Acoustics, Speech, and Signal Processing*, vol. 37, no. 7, pp. 984–995, July 1989.

[19] R. Price and E. Hofstetter, "Bounds on the volume and height distributions of the ambiguity function," *IEEE Transactions on Information Theory*, vol. 11, no. 2, pp. 207–214, April 1965.

[20] W. M. Siebert, "Studies of Woodward's uncertainty function," Electronics Research Lab., M.I.T, Cambridge Massachusetts, MA, Quarterly Progress Report, April 1958.

[21] G. S. Antonio, D. R. Fuhrmann, and F. C. Robey, "MIMO radar ambiguity functions," *IEEE Journal of Selected Topics in Signal Processing*, vol. 1, no. 1, pp. 167–177, June 2007.

[22] C.-Y. Chen and P. P. Vaidyanathan, "MIMO radar ambiguity properties and optimization using frequency-hopping waveforms," *IEEE Transactions on Signal Processing*, vol. 56, no. 12, pp. 5926–5936, December 2008.

[23] Y. I. Abramovich and G. J. Frazer, "Bounds on the volume and height distributions for the MIMO radar ambiguity function," *IEEE Signal Processing Letters*, vol. 15, pp. 505–508, 2008.

[24] V. Tarokh, N. Seshadri, and A. R. Calderbank, "Space-time codes for high data rate wireless communication: Performance criterion and code construction," *IEEE Transactions on Information Theory*, vol. 44, no. 2, pp. 744–765, Mar 1998.

[25] D. Chizhik, G. J. Foschini, M. J. Gans, and R. A. Valenzuela, "Keyholes, correlations, and capacities of multielement transmit and receive antennas," *IEEE Transactions on Wireless Communications*, vol. 1, no. 2, pp. 361–368, Apr. 2002.

[26] J.-M. Colin, "Phased array radars in France: Present and future," in *Proc. IEEE International Symposium on Phased Array Systems and Technology*, Boston, MA, 1996, pp. 458–462.

[27] A. Hassanien, S. A. Vorobyov, and A. B. Gershman, "Moving target parameters estimation in non-coherent MIMO radar systems," *IEEE Transactions on Signal Processing*, vol. 60, no. 5, pp. 2354–2361, May 2012.

[28] K. W. Forsythe, D. W. Bliss, and G. S. Fawcett, "Multiple-input multiple-output MIMO radar: Performance issues," in *Proc. Asilomar Conference on Signals, Systems, and Computers*, vol. 1, Pacific Grove, CA, November 2004, pp. 310–315.

[29] D. W. Bliss and K. W. Forsythe, "Multiple-input multiple-output MIMO radar and imaging: Degrees of freedom and resolution," in *Proc. Asilomar*

*Conference on Signals, Systems, and Computers*, vol. 1, Pacific Grove, CA, November 2003, pp. 54–59.

[30] F. Daum and J. Huang, "MIMO radar: Snake oil or good idea?" *IEEE Aerospace and Electronics Systems Magazine*, vol. 24, no. 5, pp. 8–12, May 2009.

[31] E. Brookner, "MIMO radar demystified and where it makes sense to use," in *Proc. IEEE International Symposium on Phased Array System and Technology*, Waltham, MA, October 2013, pp. 399–407.

[32] B. Friedlander, "On the relationship between MIMO and SIMO radars," *IEEE Transactions on Signal Processing*, vol. 57, no. 1, pp. 394–398, January 2009.

[33] S. A. Vorobyov and M. Lops, "Trade-offs in MIMO radar with colocated antennas," A Coruña, Spain, Tutorial in 8th IEEE Sensor Array and Multichannel Signal Processing Workshop, June 2014. [Online]. Available: http://www.gtec.udc.es/sam2014/images/sam2014/tutorials/slides_tutorial_tradeoffs_mimo_radar_sam_2014_v2.pdf

[34] D. J. Rabideau. and P. Parker, "Ubiquitous MIMO multifunction digital array radar," in *Proc. Asilomar Conference on Signals, Systems, and Computers*, vol. 1, Pacific Grove, CA, November 2003, pp. 1057–1064.

[35] R. Klemm, *Principles of space-time adaptive processing*, 3rd ed. London, United Kingdom: The Institution of Electrical Engineering and Technology, 2006.

[36] J. Ward, "Space-time adaptive processing for airborne radar," MIT Lincoln Lab., Lexington Massachusetts, MA, Technical Report 1015, December 1994.

[37] D. W. Bliss, K. W. Forsythe, S. K. Davis, G. S. Fawcett, D. J. Rabideau, L. L. Horowitz, and S. Kraut, "GMTI MIMO radar," in *Proc. International Waveform Diversity and Design Conference*, Kissimmee, FL, February 2009, pp. 118–122.

[38] K. W. Forsythe and D. W. Bliss, "Waveform correlation and optimization issues for MIMO radar," in *Proc. Asilomar Conference on Signals, Systems, and Computers*, Pacific Grove, CA, October 2005, pp. 1306–1310.

[39] B. Liu, Z. He, J. Zeng, and B. Liu, "Polyphase orthogonal code design for MIMO radar systems," in *Proc. CIE International Radar Conference*, Shanghai, China, October 2006, pp. 1–4.

[40] Y. Yang and R. S. Blum, "MIMO radar waveform design based on mutual information and minimum mean-square error estimation," *IEEE Transactions on Aerospace and Electronic Systems*, vol. 43, no. 1, pp. 330–343, January 2007.

[41] V. F. Mecca and J. L. Krolik, "Slow-time MIMO STAP with improved power efficiency," in *Proc. Asilomar Conference on Signals, Systems, and Computers*, Pacific Grove, CA, November 2007, pp. 202–206.

[42] J. Li, L. Xu, P. Stoica, K. W. Forsythe, and D. W. Bliss, "Range compression and waveform optimization for MIMO radar: A Cramér-Rao bound based study," *IEEE Transactions on Signal Processing*, vol. 56, no. 1, pp. 218–232, January 2008.

[43] C.-Y. Chen and P. P. Vaidyanathan, "MIMO radar ambiguity properties and optimization using frequency-hopping waveforms," *IEEE Transactions on Signal Processing*, vol. 56, no. 12, pp. 5926–5936, December 2008.

[44] D. J. Rabideau, "Adaptive MIMO radar waveforms," in *Proc. IEEE Radar Conference*, Rome, Italy, May 2008, pp. 1–6.

[45] J. Li, P. Stoica, and X. Zheng, "Signal synthesis and receiver design for MIMO radar imaging," *IEEE Transactions on Signal Processing*, vol. 56, no. 8, pp. 3959–3968, August 2008.

[46] C.-Y. Chen and P. P. Vaidyanathan, "MIMO radar waveform optimization with prior information of the extended target and clutter," *IEEE Transactions on Signal Processing*, vol. 57, no. 9, pp. 3533–3544, September 2009.

[47] Y. Yang, R. S. Blum, Z. He, and D. R. Fuhrmann, "MIMO radar waveform design via alternating projection," *IEEE Transactions on Signal Processing*, vol. 58, no. 3, pp. 1440–1445, March 2010.

[48] X. Song, S. Zhou, and P. Willett, "Reducing the waveform cross correlation of MIMO radar with space-time coding," *IEEE Transactions on Signal Processing*, vol. 58, no. 8, pp. 4213–4224, August 2010.

[49] B. Tang, J. Tang, and Y. Peng, "MIMO radar waveform design in colored noise based on information theory," *IEEE Transactions on Signal Processing*, vol. 58, no. 9, pp. 4684–4697, September 2010.

[50] S. Ahmed, J. S. Thompson, Y. R. Petillot, and B. Mulgrew, "Finite alphabet constant-envelope waveform design for MIMO radar," *IEEE Transactions on Signal Processing*, vol. 59, no. 11, pp. 5326–5337, November 2011.

[51] E. Grossi, M. Lops, and L. Venturino, "Robust waveform design for MIMO radars," *IEEE Transactions on Signal Processing*, vol. 59, no. 7, pp. 3262–3271, July 2011.

[52] G. Cui, H. Li, and M. Rangaswamy, "MIMO radar waveform design with constant modulus and similarity constraints," *IEEE Transactions on Signal Processing*, vol. 62, no. 2, pp. 343–353, January 2014.

[53] J. Zhang, H. Wang, and X. Zhu, "Adaptive waveform design for separated transmit/receive ULA-MIMO radar," *IEEE Transactions on Signal Processing*, vol. 58, no. 9, pp. 4936–4942, September 2010.

[54] B. Tang, J. Tang, and Y. Peng, "Waveform optimization for MIMO radar in colored noise: Further results for estimation-oriented criteria," *IEEE Transactions on Signal Processing*, vol. 60, no. 3, pp. 1517–1522, March 2012.

[55] W. Huleihel, J. Tabrikian, and R. Shavit, "Optimal adaptive waveform design for cognitive MIMO radar," *IEEE Transactions on Signal Processing*, vol. 61, no. 20, pp. 5075–5089, October 2013.

[56] S. Jardak, S. Ahmed, and M.-S. Alouini, "Generation of correlated finite alphabet waveforms using Gaussian random variables," *IEEE Transactions on Signal Processing*, vol. 62, no. 17, pp. 4587–4596, September 2014.

[57] S. Boyd and L. Vandenberghe, *Convex optimization*. New York: Cambridge University Press, 2004.

[58] Y. Li, S. A. Vorobyov, and V. Koivunen, "Generalized ambiguity function for the MIMO radar with correlated waveforms," in *Proc. IEEE International Conference on Acoustics, Speech, and Signal Processing (ICASSP)*, Florence, Italy, May 2014, pp. 5302–5306.

[59] P. M. Woodward, "Radar ambiguity analysis," Royal Radar Establishment, Ministry of Technology, Malvern, Worecs., Technical Report 731, February 1967.

[60] D. R. Fuhrmann and G. San Antonio, "Transmit beamforming for MIMO radar systems using partial signal correlation," in *Proc. Asilomar Conference on Signals, Systems, and Computers*, vol. 1, Pacific Grove, CA, November 2004, pp. 295–299.

[61] G. Hua and S. S. Abeysekera, "MIMO radar transmit beampattern design with ripple and transition band control," *IEEE Transactions on Signal Processing*, vol. 61, no. 11, pp. 2963–2974, June 2013.

[62] S. Ahmed, J. S. Thompson, Y. R. Petillot, and B. Mulgrew, "Unconstrained synthesis of covariance matrix for MIMO radar transmit beampattern," *IEEE Transactions on Signal Processing*, vol. 59, no. 8, pp. 3837–3849, August 2011.

[63] J. Lipor, S. Ahmed, and M.-S. Alouini, "Fourier-based transmit beampattern design using MIMO radar," *IEEE Transactions on Signal Processing*, vol. 62, no. 9, pp. 2226–2235, May 2014.

[64] S. Ahmed and M.-S. Alouini, "MIMO-radar waveform covariance matrix for high SINR and low side-lobe levels," *IEEE Transactions on Signal Processing*, vol. 62, no. 8, pp. 2056–2065, April 2014.

[65] S. Ahmed and M.-S. Alouini, "MIMO radar transmit beampattern design without synthesising the covariance matrix," *IEEE Transactions on Signal Processing*, vol. 62, no. 9, pp. 2278–2289, May 2014.

[66] B. Friedlander, "On transmit beamforming for MIMO radar," *IEEE Transactions on Aerospace and Electronic Systems*, vol. 48, no. 4, pp. 3376–3388, October 2012.

[67] H. Li and B. Himed, "Transmit subaperturing for MIMO radars with co-located antennas," *IEEE Journal of Selected Topics in Signal Processing*, vol. 4, no. 1, pp. 55–65, February 2010.

[68] D. Wilcox and M. Sellathurai, "On MIMO radar subarrayed transmit beamforming," *IEEE Transactions on Signal Processing*, vol. 60, no. 4, pp. 2706–2091, April 2012.

[69] A. Hassanien, M. W. Morency, A. Khabbazibasmenj, S. A. Vorobyov, J.-Y. Park, and S.-J. Kim, "Two-dimensional transmit beamforming for MOMO radar with sparse symmetric arrays," in *Proc. IEEE Radar Conference*, Ottawa, ON, Canada, April–May 2013, pp. 1–6.

[70] A. Hassanien, S. A. Vorobyov, and J.-Y. Park, "Joint transmit array interpolation and transmit beamforming for source localization in MIMO radar with arbitrary arrays," in *Proc. IEEE International Conference on Acoustics, Speech, and Signal Processing (ICASSP)*, Vancouver, BC, Canada, May 2013, pp. 4139–4143.

[71] A. Duly, D. J. Love, and J. V. Krogmeier, "Time-division beamforming for MIMO radar waveform design," *IEEE Transactions on Aerospace and Electronic Systems*, vol. 49, no. 2, pp. 1210–1223, April 2013.

[72] H. L. V. Trees, *Optimum Array Processing*. New York: Wiley, 2002.

[73] G. Xu, S. D. Silverstein, R. H. Roy, and T. Kailath, "Beamspace ESPRIT," *IEEE Transactions on Signal Processing*, vol. 42, no. 2, pp. 349–356, February 1994.

[74] E. Fishler, A. Haimovich, R. S. Blum, L. J. Cimini, D. Chizhik, and R. Valenzuela, "Spatial diversity in radars-models and detection performance," *IEEE Transactions on Signal Processing*, vol. 54, no. 3, pp. 823–838, March 2006.

[75] I. Bekkerman and J. Tabrikian, "Target detection and localization using MIMO radars and sonars," *IEEE Transactions on Signal Processing*, vol. 54, no. 10, pp. 3873–3883, October 2006.

[76] Q. He, N. H. Lehmann, R. S. Blum, and A. M. Haimovich, "MIMO radar moving target detection in homogeneous clutter," *IEEE Transactions on Aerospace and Electronic Systems*, vol. 46, no. 3, pp. 1290–1301, July 2010.

[77] A. Tajer, G. H. Jajamovich, X. Wang, and G. V. Moustakides, "Optimal joint target detection and parameter estimation by MIMO radar," *IEEE Journal of Selected Topics in Signal Processing*, vol. 4, no. 1, pp. 127–145, February 2010.

[78] G. V. Moustakides, G. H. Jajamovich, A. Tajer, and X. Wang, "Joint detection and estimation: Optimum tests and applications," *IEEE Transactions on Information Theory*, vol. 58, no. 7, pp. 4215–4229, July 2012.

[79] A. De Maio, M. Lops, and L. Venturino, "Diversity-integration tradeoffs in MIMO detection," *IEEE Transactions on Signal Processing*, vol. 56, no. 10, pp. 5051–5061, Oct 2008.

[80] C. Chong, F. Pascal, J. Ovarlez, and M. Lesturgie, "MIMO radar detection in non-Gaussian and heterogeneous clutter," vol. 4, no. 1, pp. 115–126, February 2010.

[81] S. Gogineni and A. Nehorai, "Polarimetric MIMO radar with distributed antennas for target detection," *IEEE Transactions on Signal Processing*, vol. 58, no. 3, pp. 1689–1697, March 2010.

[82] Q. He and R. S. Blum, "Diversity gain for MIMO Neyman-Pearson signal detection," *IEEE Transactions on Signal Processing*, vol. 59, no. 3, pp. 869–881, March 2011.

[83] M. Akcakaya and A. Nehorai, "MIMO radar detection and adaptive design under a phase synchronization mismatch," *IEEE Transactions on Signal Processing*, vol. 58, no. 10, pp. 4994–5005, October 2010.

[84] M. Akcakaya and A. Nehorai, "MIMO radar sensitivity analysis for target detection," *IEEE Transactions on Signal Processing*, vol. 59, no. 7, pp. 3241–3250, July 2011.

[85] P. Wang, H. Li, and B. Himed, "Moving target detection using distributed MIMO radar in clutter with nonhomogeneous power," *IEEE Transactions on Signal Processing*, vol. 59, no. 10, pp. 4809–4820, October 2011.

[86] P. Wang, H. Li, and B. Himed, "A parametric moving target detector for distributed MIMO radar in non-homogeneous environment," *IEEE Transactions on Signal Processing*, vol. 61, no. 9, pp. 2282–2294, May 2013.

[87] D. E. Hack, L. K. Patton, B. Himed, and M. A. Saville, "Detection in passive MIMO radar networks," *IEEE Transactions on Signal Processing*, vol. 62, no. 11, pp. 2999–3012, June 2014.

[88] D. E. Hack, L. K. Patton, B. Himed, and M. A. Saville, "Centralized passive MIMO radar detection without direct-path reference signals," *IEEE Transactions on Signal Processing*, vol. 62, no. 11, pp. 3013–3023, June 2014.

[89] K. W. Forsythe and D. W. Bliss, "MIMO radar waveform constraints for GMTI," *IEEE Journal of Selected Topics in Signal Processing*, vol. 4, no. 1, pp. 21–32, February 2010.

[90] J. Kantor. and S. K. Davis, "Airborne GMTI using MIMO techniques," in *Proc. IEEE Radar Conference*, Washington, DC, May 2010, pp. 1344–1349.

[91] J. M. Kantor and D. W. Bliss, "Clutter covariance matrices for GMTI MIMO radar," in *Proc. Asilomar Conference on Signals, Systems, and Computers*, Pacific Grove, CA, November 2010, pp. 1821–1826.

[92] C.-Y. Chen and P. P. Vaidyanathan, "MIMO radar space-time adaptive processing using prolate spheroidal waveform functions," *IEEE Transactions on Signal Processing*, vol. 56, no. 2, pp. 623–635, February 2008.

[93] H. Li, Y. Li, and Z. He, "MIMO radar clutter mitigation based on joint beamforming and joint domain localized processing," *EURASIP journal on wireless communications and networking (Radar and sonar networks topic)*, vol. 1, pp. 1–10, April 2013. [Online]. Available: http://jwcn.eurasipjournals.com/content/2013/1/99

[94] V. F. Mecca and J. L. Krolik, "MIMO enabled multipath clutter rank estimation," in *Proc. IEEE Radar Conference*, Pasadena, CA, May 2009, pp. 1–6.

[95] G. Wang and Y. Lu, "Clutter rank of STAP in MIMO radar with waveform diversity," *IEEE Transactions on Signal Processing*, vol. 58, no. 2, pp. 938–943, February 2010.

[96] Y. Li, S. A. Vorobyov, and A. Hassanien, "MIMO radar capability on powerful jammers suppression," in *Proc. IEEE International Conference on Acoustics, Speech, and Signal Processing (ICASSP)*, Florence, Italy, May 2014, pp. 5277–5281.

[97] Y. Li, S. A. Vorobyov, and A. Hassanien, "Robust beamforming for jammers suppression in MIMO radar," in *Proc. IEEE Radar Conference*, Cincinnati, OH, May 2014, pp. 0629–0634.

[98] Y. I. Abramovich, G. J. Frazer, and B. A. Johnson, "Noncausal adaptive spatial clutter mitigation in monostatic MIMO radar: Fundamental limitations," *IEEE Journal of Selected Topics in Signal Processing*, vol. 4, no. 1, pp. 40–54, February 2010.

[99] H. Wang and L. Cai, "On adaptive spatial-temporal processing for airborne surveillance radar systems," *IEEE Transactions on Aerospace and Electronic Systems*, vol. 30, no. 3, pp. 660–670, July 1994.

[100] D. J. Rabideau and P. Parker, "Ubiquitous MIMO multifunction digital array radar," in *Proc. Asilomar Conference on Signals, Systems, and Computers*, vol. 1, Pacific Grove, CA, November 2003, pp. 1057–1064.

[101] Y. Yu, A. P. Petropulu, and H. V. Poor, "MIMO radar using compressive sampling," *IEEE Journal of Selected Topics in Signal Processing*, vol. 4, no. 1, pp. 146–163, February 2010.

[102] M. Rossi, A. M. Haimovich, and Y. C. Eldar, "Spatial compressive sensing for MIMO radar," *IEEE Transactions on Signal Processing*, vol. 62, no. 2, pp. 419–430, January 2014.

[103] G. Krieger, "MIMO-SAR: Opportunities and pitfalls," *IEEE Transactions on Geoscience and Remote Sensing*, vol. 52, no. 5, pp. 2628–2645, May 2014.

[104] B. Correll, "Efficient spotlight SAR MIMO linear collection configurations," *IEEE Journal of Selected Topics in Signal Processing*, vol. 4, no. 1, pp. 33–39, February 2010.

[105] M. Soltanalian, H. Hu, and P. Stoica, "Single-stage transmit beamforming design for MIMO radar," *Signal Processing*, vol. 102, pp. 132–138, September 2014.

[106] W. Rowe, P. Stoica, and J. Li, "Spectrally constrained waveform design," *IEEE Signal Processing Magazine*, vol. 31, no. 3, pp. 157–162, May 2014.

[107] C. Ma, T. S. Yeo, C. S. Tan, Y. Qiang, and T. Zhang, "Receiver design for MIMO radar range sidelobes suppression," *IEEE Transactions on Signal Processing*, vol. 58, no. 10, pp. 5469–5474, Oct. 2010.

[108] G. Hua and S. S. Abeysekera, "Receiver design for range and sidelobe suppression using MIMO and phased-array radar," *IEEE Transactions on Signal Processing*, vol. 61, no. 6, pp. 1315–1326, March 2013.

[109] N. Levanon and E.Mozeson, *Radar Signals*. Hoboken, NJ: Wiley, 2004.

[110] M. Grant and S. Boyd. (2014, September) CVX: Matlab software for disciplined convex programming (version 2.1). [Online]. Available: http://cvxr.com/cvx